Genetically-modified lentiviruses that preserve microvascular function protect against late radiation damage in normal tissues

AA Khan[1,2], JT Paget[1,2], M McLaughlin[1], JN Kyula[1], MJ Wilkinson[1], T Pencavel[1], D Mansfield[1], V Roulstone[1], R Seth[1], M Halle[3], N Somaiah[1], J Boult[2], SP Robinson[4], HS Pandha[5], RG Vile[6], AA Melcher[7], PA Harris[2] and KJ Harrington[1].

Affiliations:

[1]Targeted Therapy Team, Division of Radiotherapy and Imaging, The Institute of Cancer Research, London

[2]Department of Plastic Surgery, The Royal Marsden Hospital, London

[3]Department of Molecular Medicine and Surgery, Section of Plastic Surgery, Karolinska Institute, and Department of Reconstructive Plastic Surgery, Karolinska University Hospital, Stockholm, Sweden

[4]Magnetic Resonance Team, Division of Radiotherapy and Imaging, The Institute of Cancer Research, London

[5]Postgraduate Medical School, The University of Surrey, Guildford

[6]Molecular Medicine Program, Mayo Clinic, Rochester

[7]Translational Immunotherapy Team, Division of Radiotherapy and Imaging, The Institute of Cancer Research, London

One Sentence Summary:

A combination of virally-delivered *SOD2* and *CTGF* gene therapies can protect non-cancerous tissues from the long-term side effects of radiotherapy

Abstract: Improvements in cancer survival mean that long-term toxicities are being increasingly recognised that contribute to the morbidity of cancer survivorship. Late adverse effects (LAEs) in normal tissues after radiotherapy (RT) are characterized by vascular dysfunction and fibrosis leading to volume loss and tissue contracture. For example, irradiation of free flaps used for immediate breast reconstruction after mastectomy results in LAEs that distort the reconstructed breast, necessitating salvage reconstruction long after cancer treatment is complete. We evaluated the efficacy of lentiviral superoxide dismutase 2 (LVSOD2) and connective tissue growth factor (CTGF) shRNA in reducing the severity of LAEs using a novel animal model of free flap LAEs. Vectors were delivered by intra-arterial injection, *ex vivo*, to target the vascular compartment. LVSOD2 and LVshCTGF monotherapy prior to irradiation resulted in significant preservation of flap volume or reduction in skin contracture, respectively. Flaps transduced with combination therapy experienced significant improvements in both volume loss and skin contracture. Both therapies significantly reduced the fibrotic burden after irradiation. LAEs were associated with impaired vascular perfusion, loss of endothelial permeability and stromal hypoxia that were further reversed in the described treatment model. Using a model of tumour recurrence within transduced flaps we showed that *SOD2* over-expression in normal tissues did not compromise the cytotoxic efficacy of RT against tumour cells but instead, paradoxically, appeared to enhance it. LVSOD2 and LVshCTGF combination therapy by targeted, intra-vascular delivery reduced LAE severities in normal tissues without compromising the efficacy of RT and warrants translational evaluation as a free flap-targeted gene therapy.

Introduction

Ever improving cancer survival means that the long-term toxicities of cancer treatments that contribute to the morbidity of cancer survivorship are being increasingly recognized. For example, for women diagnosed with small screen-detected breast cancers, it is the late complications of radiotherapy, rather than the risk of loco-regional recurrence(*1, 2*), that are the dominant hazard. Late adverse effects (LAEs) in the breast include breast shrinkage, hardening, discomfort and skin changes. These changes (*3-7*) also occur in breasts that have been reconstructed with free flaps after mastectomy and augur a poorer long-term aesthetic outcome. Re-operation rates for flaps affected in this manner are significant and, in some cases, salvage reconstruction with a second free flap remains the only option. Such late adverse effects (LAEs) incur significant physical and psychological morbidity in cancer survivorship. Therefore, if adjuvant RT may be required, and when the surgical defect allows, free flap reconstructions are delayed until 6 months post-RT (e.g. delayed breast reconstruction post-mastectomy)(*8*). However, such delays incur more operative procedures(*9*), multiple hospital admissions for the patient(*10*), and, result in aesthetically inferior reconstructive outcomes compared to immediate reconstructions (*11, 12*). Consequently, conferring radioprotection to a free flap offers the clinical benefit of allowing patients undergoing reconstructions after cancer excision to have an earlier reconstruction, which is more durable against the adverse effects of adjuvant therapies.

Irradiation of the vasculature has been shown to cause endothelial dysfunction, sustained inflammation, pruning of the vascular architecture and a pro-thrombotic milieu defined by over-expression of plasminogen activator inihibitor 1 (PAI-1)(*13-15*). It is postulated that the dense fibrotic reaction in LAEs may represent aberrant, dysregulated, compensatory responses to tissue hypoxia caused by vascular damage(*16*). RT-induced reactive oxygen species (ROS) are implicated(*17, 18*) in the activation of pro-fibrotic pathways, such as TGF-β1 and connective tissue growth factor (CTGF), and appear to be central to the development of LAEs. Specifically, altered expression of cellular adhesion molecules (VCAM1/ICAM1)(*19*), endothelial-to-mesenchymal transition (Endo-MT)(*15, 20-22*) and over-expression of PAI-1(*13-15*) are thought to be central mechanisms that instigate the development of LAEs. ROS are normally inactivated by the enzyme superoxide dismutase (SOD), which exists in cytoplasmic (SOD1), mitochondrial (SOD2) and extra-cellular (SOD3) forms. *SOD2* gene therapy radioprotects normal cells *in vitro* and *in vivo*(*19, 23-30*) and has been tested in a phase I clinical trial(*31*). *SOD2* gene therapy represents an attractive therapeutic strategy as it targets an early step in the pathophysiological cascade from irradiation to LAEs. CTGF, a downstream effector of TGFβ1 signaling, is over-expressed in radiation-induced fibrosis(*35-37*) and other pathological fibrotic states(*38-40*). Therefore, we sought to develop a radioprotective therapy to target both oxidative stress (SOD2) and fibrotic (CTGF) pathways.

The challenge in delivering radioprotective therapies is to target, specifically, normal tissues and not those that may harbor microscopic residual disease. Clinically, such an opportunity arises when performing free tissue transfer, for example in the case of immediate breast reconstruction following mastectomy (*41-43*). Free flaps are composite blocks of tissue harvested from distant donor sites on their supplying blood vessels. Radioprotective gene therapy strategies using plasmid/liposomal, and virally-delivered, SOD2 have been reported previously (*24, 31-34*) where vectors are delivered either directly to target organs, or, delivered intravenously. Due to the central role of the vascular compartment in the development of LAEs we, therefore, sought to protect selectively the vasculature of normal tissues by delivering radioprotective vectors intra-arterially into flaps during the ischemic interval. We hypothesized that over-expressing SOD2 and silencing CTGF would reduce the severity of LAEs in irradiated

normal tissues without compromising the anti-tumour efficacy of RT. We sought to investigate this using a free flap gene therapy model(*43-48*) as it permits exquisite anatomic control of viral delivery and because of its potential for subsequent translation.

We show that free flap irradiation causes characteristic contracture and volume loss, akin to those seen in the clinical context. We show that these changes are due to irreversible damage in the vascular compartment that leads to the generation of tissue hypoxia and fibrosis. We generate therapeutic lentiviral vectors that mediate durable transgene expression *in vivo* and show that SOD2 over-expression and CTGF silencing achieve differential effects in ameliorating LAEs within irradiated flaps. We demonstrate that SOD2 monotherapy preserves flap volume by maintaining vascular architecture and function, whereas anti-CTGF monotherapy reduces post-RT cutaneous contracture. Combination therapy with both vectors protects irradiated flaps against both volume loss and flap contracture. Finally, we show that SOD2 over-expression in normal tissues does not compromise the efficacy of RT and may indeed enhance it.

Results

Irradiation of SIEA flaps with 50 Gy in 3 fractions produces a clinically-relevant LAE phenotype characterized by SOD2 depletion, CTGF over-expression and fibrosis

We report a previously undescribed model of free flap irradiation using the superficial inferior epigastric artery (SIEA) flap in rodents (fig. S1) that we developed specifically to test our hypotheses. In brief, we trialed 3 biologically-equivalent fractionation schedules and characterized the LAEs that developed *in vivo* after irradiation (fig. S1). SIEA flaps irradiated with 50 Gy/3 fractions developed a clinically-relevant LAE phenotype (fig. S1) characterized by skin paddle contracture (figure 1A. i-iv), volume loss and pathognomonic skin changes (altered pigmentation and telangiectasia). Skin paddle surface areas were significantly reduced in irradiated flaps compared to un-irradiated controls (figure 1 A and B). Irradiated flaps exhibited acute RT-induced toxicities (fig. S1) ranging from dry desquamation to confluent, moist desquamation. Acute toxicities (scored using the Radiotherapy Oncology Group (RTOG) criteria(*49*)) were evident at day 7, peaked at day 14 post-RT and resolved by 35 days (figure 1.C.i.). Irradiated flaps attained progressively higher scores on the RTOG LAE criteria (figure 1.C.ii.). Late RTOG scores stabilized by 140 days post-RT with irradiated flaps attaining a mean score 5.85 (SEM: 0.10) at 180 days. LAEs were first evident in the skin followed by the subcutaneous tissues and, ultimately, the knee joint (figure 1.C.iii.). Mean passive ROM at irradiated knee joints was significantly reduced compared to non-irradiated controls (figure 1.C iv.). Magnetic resonance imaging (MRI) of irradiated, and matched un-irradiated controls *in vivo* revealed significant reductions in flap volume at 6 months (figure 1.D.i-iii).

We observed CTGF over-expression (figure 1.E.i and 1.G.i-iii) and functional SOD2 depletion (figure 1.E.ii) in irradiated flaps. Western blot analyses demonstrated a reduction in SOD2 protein levels and activation of Wnt signaling in irradiated flaps (figure 1.F). Histological analysis (Masson's trichrome staining) revealed a dense fibrotic reaction and greater fat necrosis in irradiated flaps (figure 1.G.i-iii). RT-QPCR analyses demonstrated significant reductions in *CTGF* and *COL3a1* ($p<0.05$) expression and increased *COL1a2* gene expression ($p<0.001$) (figure 1.H.i-iii). Taken together, these data suggest that the LAE phenotype in our model exhibits clinical, anatomical, volumetric and biological changes similar to those seen in a clinical setting.

Irradiated flaps exhibit abnormal vascular function characterized by loss of endothelial function and fibrosis

Quantitative functional imaging of irradiated and matched un-irradiated flaps demonstrated significant changes in the MRI transverse relaxation rate R_2* of flap tissues following irradiation (figure 2.A). Briefly, the presence of paramagnetic deoxyhaemoglobin in erythrocytes creates magnetic susceptibility perturbations around blood vessels, increasing R_2* of the surrounding tissue in proportion to the tissue deoxyhaemoglobin concentration. This non-invasive approach offers a sensitive method of monitoring the dynamics of vascular modeling, function and regression *in vivo(50-52)*. Prior to irradiation, flaps situated on the left hind limb (that were due to be irradiated) had a faster R_2* than flaps on the contralateral, control hind limb ($p<0.05$) (figure 2.B.i). In irradiated flaps, the mean absolute R_2* decreased progressively and, normalized to pre-RT R_2* values, stabilized at 56% at 6 months post-RT (figure 2.B.ii). Two-way ANOVA showed these changes to be statistically significant ($p=0.0004$) and post-hoc analyses revealed that irradiated flaps had significantly slower R_2* values from 1 month post-RT ($p<0.001$) (figure 2.Bb.ii) onwards.

To correlate vascular function and structure, we performed immunofluorescence analyses using markers for perfused (functional) blood vessels (Hoechst 33342), vascular permeability (Evans blue) and hypoxia (pimonidazole adduct formation). Irradiated flaps demonstrated significant reductions in functional vasculature (control 34.9% v. irradiated 16.5%; $p < 0.001$) and vascular permeability (control 19.4% v. irradiated 3.8%; $p < 0.0001$) (figure 2.c-f), and greater hypoxia within the stromal compartment (control 5.2% v. irradiated 16.7%; $p< 0.001$) (figures 2.C., D. and G.). Areas of hypoxia were observed surrounding vessels exhibiting a dense fibrotic reaction (figure 2.G.).

In summary, LAEs are associated with vascular dysfunction characterized by a reduction in R_2* indicating impaired haemodynamic vasculature. This dysfunction is associated with loss of patent vasculature, peri-vascular fibrosis and tissue hypoxia.

Development and validation of LVSOD2 and LVshCTGF in vitro and the durability of lentivirally-delivered transgene expression in vivo

Having demonstrated SOD2 depletion in LAEs *in vivo*, we investigated how soon after irradiation this occurred. A time-course study of irradiated fibroblasts showed early and RT dose-dependent reductions in SOD2 activity (figure 3.A.). We subsequently generated stable SOD2-overexpressing fibroblast cell lines and showed that SOD2 activity could be significantly increased from basal levels (fig. S2). SOD2 overexpressing stable cells (RF-LVSOD2) retained significantly ($p < 0.001$) greater SOD2 activity than both naïve cells and stable cells generated by infection with a control vector (RF-LVGFP) post-RT with 8 or 16 Gy (figure 3.B). To investigate whether this survival effect was apparent across fractionated, in addition to, single-fraction doses we performed MTT assays at 120 hours in endothelial cells (YPEN1) after irradiation with 3 biologically-equivalent fractionation doses (5 Gy single fraction, 6.4 Gy/2 fractions and 7.2 Gy/3 fractions). We observed significant increases in cell survival across all fractionation schedules (figure 3.C) and further confirmed this using 3D spheroid assays (YPEN1) (figure 3.D) where we observed significantly greater preservation of spheroid volume following RT in cells over-expressing SOD2 (YPEN SOD2). To investigate whether this survival benefit was specific to SOD2 over-expression we performed transient *SOD2* knock-down in YPEN1 cells using siRNA 48 hours prior to RT (figure 3.E). We observed that *SOD2* knock-down resulted in reversal of the survival benefit observed previously and PCR demonstrated significant reductions in *SOD2* gene expression using this strategy. Clonogenic assays in tumour cell lines (HeLa and FaDu) demonstrated inconsistent differences in survival following irradiation between cells over-expressing SOD2 and controls (figure 3.G. and H.) ($p<0.05$). Finally, to investigate whether the radioprotective effects we had observed were being mediated through the mitochondrial, or cytosolic, localization of SOD2 we performed immunofluorescent staining for SOD2 in transfected cells using anti-mitochondrial (cytochrome C oxidase: MTCO1) antibodies (figure 3.I). We observed greater SOD2 expression in cells infected with LVSOD2 (figure 3.I.ii) and that SOD2 expression co-localised to the mitochondrial, rather than the cytosolic, compartment. To confirm this, we harvested lysate from mitochondrial and cytosolic compartments of cells over-expressing SOD2 in a stable manner and relevant controls (figure 3.I.iii) for analysis of biochemical SOD2 activity. We observed that SOD2 activity was significantly increased in the mitochondrial compartment ($p<0.01$) of cells over-expressing SOD2 but not in the cytosolic compartment.

Briefly, using a second generation lentiviral backbone, we cloned several plasmids encoding shRNA sequences targeted against rat CTGF and used these to generate a battery of lentiviral particles by transfection of HEK 293T cells. Lentiviral particles were used to create

stable cell lines (rat fibroblasts) and CTGF knock-down was quantified by ELISA using *in vitro* models of basal and stimulated (+ TGF-β1) CTGF expression (supplementary figure 2.C. and D.). We identified a lead candidate shRNA that knocked down both basal, and stimulated, CTGF to approximately 50% of that seen in naïve, control cells and this was used for further *in vivo* investigation.

To investigate whether SOD2 over-expression and CTGF knock-down could be achieved *in vivo*, we infected SIEA flaps with LVSOD2 (10^8 TUs) and LVshCTGF (10^8 TUs) and harvested flap tissues 30 days post-operatively - the time point at which flaps would have been irradiated. We found increased SOD2 protein expression in the SIEA vascular pedicle of LVSOD2-infected flaps compared to matched, contralateral, control SIEA flap vessels (figure 3.J. i and ii). Using a biochemical activity assay, we confirmed significantly greater SOD2 activity in LVSOD2-infected flaps compared to controls ($P < 0.001$) (figure 3.J.iii). Flaps infected concomitantly with LVSOD2 and LVshCTGF showed significantly reduced CTGF levels compared to controls and those infected with LVSOD2 only ($p < 0.01$) (figure 3.J.iv). As our therapeutic strategy aimed to target the vascular system, we sought to demonstrate increased SOD2 activity within the vascular compartment. We, therefore, dissected out the vascular pedicle to the flap (SIEA and SIEV) and extracted RNA and protein from this tissue. RT-QPCR demonstrated significant *SOD2* transcript over-expression (figure 3.K) in flaps infected with LVSOD2 compared to sham controls. This was further validated by functional SOD2 assay (figure 3.L) that showed LVSOD2-infected pedicles had greater ROS scavenging activity compared to controls.

Due to the duration over which LAEs manifest in our model, we investigated the durability of transgene expression *in vivo*. SIEA flaps were infected with a GFP-expressing lentiviral vector (LVeGFP) and flap tissues were harvested at 180 days post-infection. We observed sustained GFP expression in large (SIEA, SIEV) and small vessels (figure 3.M. i-vi). In addition, we observed GFP expression in extra-vascular tissues, notably adipose (figures 3.E.vii and viii), skin, muscle and nerve (fig. S2). To quantify viral DNA in flap tissues, we performed Q-PCR on genomic DNA extracted from flap tissues 180 days post-infection and found 10^4 relative copies of the lentiviral *gag* gene per 100 ng of DNA (figure 3.N.).

Combinatorial gene therapy with LVSOD2 and LVshCTGF in free flaps mitigates the LAEs of radiotherapy

SIEA flaps infected with LVSOD2 and/or LVshCTGF showed significant improvements in LAE phenotype, skin paddle contracture, acute and late toxicity scores and flap volume retention (figure 4). Flaps transduced with LVSOD2 and LVshCTGF exhibited (figure 4.A.i-v) less pigmentation change and contracture, even in the presence of typical LAE changes (such as telangiectasia) arising in adjacent skin, outside the zone of viral vector delivery (figure 4.a.iii (red arrows)). There was no mitigation of RT-induced effects with the scrambled vector control (LVsh-scram) (figure 4.A.v). Skin paddle contracture was improved significantly in flaps transduced with both LVSOD2 (relative surface area: 53.8%; $p < 0.05$) and LVshCTGF monotherapy (relative surface area: 70.8%; $p < 0.0001$) compared to controls (PBS sham (relative surface area: 33.9%) and LVsh-scram (relative surface area: 25.4%). The greatest improvement occurred in the LVSOD2 and LVshCTGF combination cohort (relative surface area: 86.5%; $p < 0.0001$) (figure 4.A.vi and vii).

Flaps transduced with LVSOD2, alone or in combination, exhibited significant reductions ($p<0.01$) in the duration, but not maximum severity, of acute toxicities post-RT (figure 4.B.). At 180 days, SIEA flaps infected with LVSOD2, alone or in combination, showed sustained and significant reductions in RTOG severity scores ($p < 0.05$) (figure 4.C.i and iii). Flaps infected with LV-shCTGF demonstrated early improvements in RTOG severity scores ($p< 0.05$) but these were not sustained (figure 4.C.ii). Analysis of the RTOG component scores for skin, subcutaneous tissues and joint showed that LVSOD2-infected flaps exhibited significant preservation of subcutaneous volume (figure 4.C.ii and vi.) and a more modest improvement in skin severity scores. Conversely, LVshCTGF-infected flaps had greater improvements in skin component scores but scored poorly with regards to subcutaneous volume loss (figure 4.C.iv). All cohorts scored maximum severity points for joint-related changes, as would be expected given that joint tissues were extrinsic to the zone of vector delivery. These data demonstrate differential improvements in skin paddle contracture and flap volume loss attributable to LVshCTGF and LVSOD2, respectively, suggesting different mechanisms for RT-induced skin paddle contracture and volume loss. Thus, combination therapy with both LVSOD2 and LVshCTGF is required for the greatest radioprotective effect.

In vivo MRI demonstrated significant improvements in flap volume only in those flaps transduced with LVSOD2, either alone or in combination ($p<0.0001$) (figure 4.D.i-vi) compared to controls. Analysis of functional MRI data also demonstrated that flaps transduced with LVSOD2, alone or in combination, demonstrated normalization of R_2* towards that seen in unirradiated flaps ($p=0.0004$) (figure 4.D.vii). Taken together, these data support the earlier findings that LVSOD2 therapy is responsible for the preservation of flap volume post-RT and that this is associated with preservation of the vasculature.

To investigate whether SOD2 levels remained elevated in irradiated flaps, Western blot analyses were performed (figure 5.A.) and showed preservation of SOD2 protein levels in irradiated flaps infected with LVSOD2 compared to those infected with LVshCTGF and controls.

Masson's trichrome staining of irradiated flaps demonstrated greater fibrosis in control flaps compared to those infected with LVSOD2 and LVshCTGF, either alone or in combination ($p<0.0001$). Post-hoc analysis revealed that flaps infected with LVSOD2 (% fibrosis 7.8%) and LVshCTGF (% fibrosis 7.9%) monotherapy exhibited significantly less fibrosis post-irradiation ($p<0.0001$) compared to sham (% fibrosis 35.0%) and scrambled controls (% fibrosis 29.4%). Flaps infected with LVSOD2 plus LVshCTGF combination therapy exhibited significantly less fibrosis (% fibrosis 1.7%) than those receiving either agent as a monotherapy ($p<0.05$) and the burden of fibrosis was found to be no different compared to unirradiated flaps ($p>0.05$) (figure 5.B. and C.i.). Reverse transcriptase Q-PCR (RT-QPCR) revealed significant reductions in *col1a2* gene expression in flaps infected with LVSOD2, either alone or in combination ($p<0.01$) compared to controls (figure 5.C.ii). Interestingly, flaps infected with LVshCTGF alone did not demonstrate reduced *col1a2* gene expression despite exhibiting reductions in fibrosis compared to sham and scrambled controls (fig.5.C.ii).

Functional vascular analyses demonstrated reductions in perfused vasculature (Hoechst 33342) and permeability (Evans blue), and the presence of stromal hypoxia (pimonidazole) in

irradiated flaps, as described earlier. However, flaps infected with LVSOD2, either alone or in combination, demonstrated significantly greater Hoechst 33342 uptake ($p<0.0001$), Evans blue leakage ($p<0.0001$) and significantly less pimonidazole adduct formation ($p<0.0001$) compared to sham and scrambled controls (figure 5.D. and E.). Flaps infected with LVshCTGF alone demonstrated levels of Hoechst 33342 uptake not dissimilar to sham (PBS) controls but significantly greater than scrambled controls ($p<0.01$) and similar levels of pimonidazole staining compared to irradiated, but untreated, flaps. However, LVshCTGF-infected flaps exhibited significantly greater Evans blue leakage compared to irradiated controls, but significantly less staining than flaps infected with LVSOD2 (either alone or in combination)($p<0.001$) and un-irradiated controls ($p<0.0001$) (figure 5.D. and E.). Taken together, these data suggest that LVSOD2 protects against the development of LAEs through preservation of vascular function as demonstrated by the observed improvements in perfused vasculature and vascular permeability following irradiation, and the associated reduction in hypoxia. The contribution of LVshCTGF in this context is that of preserving vascular permeability although this is not to the same degree as that observed with LVSOD2 therapy and does not correlate with a reduction in the development of tissue hypoxia following irradiation. To investigate to what extent both viral vectors co-localized within the vascular compartment of the flap we performed multi-plexed immunofluorescent staining for GFP (LVshCTGF) and RFP (LVSOD2) (figure 5.F). We observed dual infection of endothelial cells with both vectors (figure 5.F) but also observed extra-vascular co-localization. Cells that had been infected with a single vector only were infrequent.

LVSOD2 therapy in normal tissues does not compromise the anti-tumour efficacy of radiotherapy

Because of concerns that SOD2 over-expression in stably transduced flap tissues might lead to increased survival of microscopic residual disease (MiRD) through release of SOD2, we performed conditioned medium experiments taking supernatant from HeLa-LVSOD2 "producer" cells and using it to inoculate naïve HeLa "target" cells. We found no evidence that SOD2 was transmitted between cell types (figure 6.A.).

To elucidate the effects of tumour bed irradiation through a flap expressing radioprotective genes, we developed an *in vivo* model of tumour recurrence within rodent SIEA flaps. Briefly, flaps were transduced (PBS sham, LVSOD2 and LVeGFP; n = 5 per group) and, at a later date, engrafted with syngeneic MatBIII tumour cells 26 days post-operatively (figure 6.B). Established tumours were irradiated (20 Gy/5 fx) and tumour growth and animal survival were recorded. Untreated tumours growing in sham-transduced flaps grew rapidly to humane end-point. Tumours irradiated in sham-transduced flaps exhibited growth delay, but 4 of 5 tumours ultimately grew to humane end-point. Tumours irradiated in LVSOD2-infected flaps exhibited significant reductions in tumour growth (figure 6.C.). Of this group, 4 of 5 tumours achieved complete remission to 40 days (figure. 6.D.iii.). We repeated the experiment using a control lentiviral vector (LVeGFP) and tumour growth closely mirrored that seen in the sham-transduced group (figure. 6.D.iv). Survival to humane end point was also significantly prolonged in the LVSOD2 group compared to sham- and LVeGFP-transduced controls ($p < 0.0001$) (figure 6.E.).

In summary, these data support our hypothesis that SOD2-mediated radioprotection of normal tissues does not compromise the anti-tumour efficacy of RT on MiRD. Indeed, normal tissue radioprotection may modulate favourably the RT response through manipulation of the normal tissue microenvironment.

Discussion

The development of LAEs within normal tissues poses a challenging clinical problem, irrespective of the tissues in which they may arise. The prevalence of LAEs in irradiated free flaps has been reported to be as high as 60% in some series(*6*). Therefore, where the option exists, surgeons frequently choose to defer reconstruction until after the completion of radiotherapy. LAEs in irradiated flaps have a significant adverse impact on cancer survivorship by necessitating further surgery years after cancer treatment is complete. Protecting free flaps from the adverse effects of radiotherapy represents an attractive therapeutic strategy. In conjunction with the clinical imperative, the technical procedure of performing a free flap also offers a distinct therapeutic window for the delivery of viral gene therapies in a manner that is exquisitely anatomically controlled. This concept of "free flap gene therapy" was first described using a liposomal vector carrying the *VEGF* gene(*53*) but later characterized extensively by Gurtner's group(*45, 46*). Unlike systemically-delivered viral gene therapies, free flap gene therapy has fewer potential barriers to success because the viral vectors are not exposed to the systemic circulation, thereby reducing specific and non-specific immune neutralisation, they by-pass the reticuloendothelial system and can be delivered in high titres exclusively to target tissues(*54*). In the current work, therefore, we used a combinatorial radioprotective strategy by directing lentivirally-delivered transgenes into flap tissues *ex vivo* before irradiation.

Radiation-induced reactive oxygen species (ROS) mediate their effects over a hyperacute time frame and SOD2 over-expression represents a very proximal point for therapeutic blockade of LAEs(*19, 23-26, 30, 32*). Previous work has demonstrated the efficacy of a *SOD2* gene therapy strategy delivered topically as a plasmid/liposome (*23, 25, 26, 31, 55*), packaged in an adenoviral vector (*30*) or delivered systemically (*34, 56*). In contrast, CTGF exerts its effects over a more prolonged time course, as seen by its involvement in fibrotic disease states, including cirrhosis, systemic sclerosis, pulmonary, renal fibrosis, and chronic transplant rejection. CTGF over-expression has been demonstrated in tissues exhibiting LAEs, but this has largely been independent of raised TGF-β1 expression and Smad signaling(*18, 37*). Alternative signaling mechanisms, such as Rho/ROCK, drive CTGF expression in this context, and pharmacological intervention (e.g. statins as Rho/ROCK inhibitors) has reversed the established LAE phenotype in animal models(*57, 58*). CTGF-targeted therapies aim to reduce the drive to fibrosis and, thus, represent a distal therapeutic blockade of LAEs (*40*). Having observed reductions in SOD2 expression/activity and CTGF over-expression in our rodent model, we designed a dual-targeted preventative approach to augment the oxidative stress response and block fibrosis.

We developed a novel model of free flap irradiation in order to test our hypotheses. We showed that irradiating flaps with 50 Gy/3 fractions recapitulated the clinical development of LAEs with prominent contracture, volume loss, fibrosis and activation of relevant signaling pathways (figure 1). In addition, we were able to show that LAEs were associated with impaired vascular function as quantified by loss of perfused vasculature, vascular permeability and the subsequent development of stromal hypoxia (figure 2). As such, this model represents an excellent platform in which to test preventative and therapeutic strategies. Subsequently, we generated and validated LVSOD2 and LVshCTGF vectors *in vitro* and confirmed that mitochondrial SOD2 over-expression is associated with increased survival post-radiotherapy *in*

vitro (figure 3. A-F and I) across a range of fractionation schedules. Using transient knock-down of *SOD2* gene expression with siRNA, we demonstrated a reversal of the radioprotective effect of SOD2 over-expression (figure 3.E). In validating this strategy *in vivo,* we were able to demonstrate that SOD2 is over-expressed and CTGF concentrations are reduced following lentiviral infection (figure 3. J-L), SOD2 over-expression particularly is evident within the vascular compartment of flaps (figure 3. K and L) and that infection with a combination of lentiviral vectors leads to co-localization of infectivity (figure 5.F).

Importantly, by using conditioned medium experiments, we were able to prove that over-expression of mitochondrial SOD (SOD2) in normal tissues of the flap would not provide a soluble, released mediator of radioprotection in neighbouring tumour cells (Figure 6.A). Infection with LVSOD2 and LVshCTGF were shown to result in functional gains in SOD2 activity and reductions in CTGF concentration, respectively. We then developed a model of tumour (rodent breast adenocarcinoma) recurrence in SIEA flaps infected with LVSOD2 or a vector control (LVeGFP) in order to test the efficacy of irradiating tumour cells in the context of a radioprotected normal microenvironment (figure 6.B.). Interestingly, tumours growing in LVSOD2-infected flaps had a more favourable response to radiotherapy (median survival not reached) compared to those irradiated in sham-infected (PBS) flaps (median survival = 27 days). To investigate whether this might be due to enhanced immune surveillance within flap tissues, as a non-specific effect of lentiviral infection, we repeated the experiment with a vector control (LVeGFP) and observed similar disease progression to that seen in the sham cohort (median survival = 25 days) (figure 6). These data prove that radioprotecting normal flap tissues will not compromise the anti-tumour efficacy of radiotherapy, and indeed may modulate favourably the tumour microenvironment to enhance treatment efficacy. The mechanisms underlying this observation are at present unclear, and the subject of ongoing work, however, previous authors have reported the direct, anti-tumour effects of SOD2 over-expression that are thought to be mediated by metabolic intermediaries (e.g. superoxide or hydrogen peroxide), inhibition of vascular endothelial growth factor and epigenetic modification (*59-63*). However, in the context of our model, where tumours are not directly infected with LVSOD2, we favour an immunological hypothesis. That is, in the presence of normal tissue radioprotection with LVSOD2, fewer distracting, immunological signals are generated after RT leading the immune response to target those cells that are not radioprotected, i.e. tumor cells.

We monitored the durability of transgene expression in lentivirally-infected free flaps using GFP and saw robust levels of gene expression out to 180 days. We tested LVSOD2 and LVshCTGF, both as mono- and combination therapies in our LAE model. Although LVSOD2 and LVshCTGF individually improved the LAE phenotype, the greatest gains, as judged by clinical parameters, were achieved by combining the two agents. Interestingly, the two vectors appeared to exert differential improvements on the LAE phenotype: LVSOD2 was more efficacious in preserving flap volume and vascular function, whilst LVshCTGF was more effective in preventing skin/flap contracture (figure 4). These improvements were associated with significant reductions in fibrosis when delivered as monotherapies, and in an additive fashion when used as a combination approach (figure 5. B. and C.). Finally, we were able to confirm that improvements in flap volume with LVSOD2 therapy (either alone or in combination) were due to preservation of vascular function and the subsequent reduction in stromal hypoxia (figure 5. D. and E.). The contribution of CTGF knock-down to the mitigation of LAEs is interesting and is most evident when considering flap skin paddle contracture (figure 4. A.) and stromal fibrosis (figure 5.B. and C.). From the functional vascular analysis, LVshCTGF monotherapy resulted in significant improvements in vascular permeability (figure

5. E. ii), but this did not result in significant reductions in stromal hypoxia compared to controls (figure 5. E. iii). Taken together, these data suggest that CTGF blockade reduces both stromal and peri-vascular fibrosis but this, on its own, is insufficient to prevent the development of hypoxia, presumably as a result of impaired endothelial function that LVshCTGF monotherapy does not prevent.

Structurally, irradiation of the vasculature causes a dose-dependent destruction of blood vessels, which particularly affects the microvasculature(*64-68*). The loss of vascular density increases the distance between functioning vessels, meaning that some parenchymal tissues fail to be perfused. In the longer-term, irradiated blood vessels become thicker, primarily due to intimal thickening, and develop a propensity to atherosclerosis. It has been proposed(*69*) that the cumulative effects of endothelial dysfunction and death, after irradiation, lead to a breakdown in transport functions and trigger a self-propagating cycle of inflammation (mediated by cytokines such as tumour necrosis factor alpha (TNF-α) and ROS), cellular proliferation and fibrosis. At a microvascular level, previous studies have shown sustained, acute inflammation of vasculature following irradiation associated with nuclear factor kappa-B (NF κB) activation and over-expression of plasminogen activator inhibitor 1 (PAI-1) (*13*, *15*), as well as differential regulation of *SOD2* expression in irradiated arteries(*70*). Furthermore, elegant studies using recombinant mice, homozygous deletion negative for endothelial adhesion molecules (ICAM1, VCAM1, E-selectin and L-selectin), (*71*) have shown that L-selectin$^{-/-}$ mice had increased survival and reduced pulmonary fibrosis after thoracic irradiation. This work demonstrates a central role for the endothelial compartment in mediating cellular responses to RT and future work might seek to investigate how SOD2 over-expression modulates adhesion molecule expression to regulate differentially immune and haematopoietic cell trafficking after RT. In the current model, loss of vascular function resulted in stromal hypoxia that was most evident around vessels exhibiting a dense fibrotic reaction (figure 2. G.). We postulate that perivascular fibrosis observed in LAEs may, therefore, represent a dysregulated compensatory mechanism to overcome the loss of microvascular function. The preservation of vascular function, through *SOD2* over-expression after radiotherapy, had a significant effect in preserving the normal phenotype even as a single agent therapy. This may be due to the fact that intra-arterial delivery of a viral vector, which is the most effective way of achieving diffuse transgene expression across all flap tissues(*48*), achieves the greatest multiplicity of infection (MOI) for the cells of the vascular tree as they are the cells of first contact for the viral particles.

In conclusion, these data provide preclinical evidence to support a combination strategy to augment proximal, oxidative stress responses within the vascular compartment, and mitigate distal, end-stage fibrosis reactions in post-radiation LAEs in irradiated free flaps. These therapeutic goals can be combined additively and can be achieved without compromising the anti-tumour efficacy of radiotherapy. Translation of this concept is feasible within the constraints of the technical considerations of free flap surgery and may allow for patients to be offered earlier reconstructions that are more durable against the side effects of adjuvant cancer therapies.

Materials and Methods

Surgical model

Under inhalational anaesthesia, superficial inferior epigastric artery (SIEA) flaps were raised in Fischer (F344) male rats (250g) (Harlan Laboratories, Huntingdon, UK) as described previously(*72*). Viral vectors ($1x10^8$ transducing units (TUs)) were delivered into flaps by intra-arterial injection through a 27G cannula along with 1 μg recombinant rat vascular endothelial growth factor A (VEGF-A), in a total injection volume of 500 μL. Viral particles were left to incubate for 50 minutes before the vascular compartment was flushed through and vascular anastomoses performed to re-establish blood flow within the flap. The flap was inset into the ventral hind limb of the animal and the animal recovered. All animal experiments were conducted in accordance with institutional and Home Office (PL: 70/7947) regulations.

SIEA flap irradiation

Flap irradiation was performed 30 days post-operatively under anaesthesia (i.p. 10 mg/mL fentanyl and 5 mg/mL midazolam). Rats were placed in a radioprotective lead shield (6 mm) containing an aperture under which the flap could be positioned. Irradiation was performed using an orthovoltage (250 kV) X-ray machine (AGO, Reading, UK). Irradiation was performed at 250 kV, 11 milliamps and at a dose rate of 4.5 Gy/min. Animals were maintained for serial clinical measurements for skin paddle contracture and RTOG severity scores for 180 days post-irradiation. At 180 days, flap tissues and contralateral control tissues were harvested for analyses under terminal anesthesia.

Tumour recurrence model

Animals underwent SIEA flap procedures as described above. Rat MatB III breast adenocarcinoma cells (ATCC, Teddington, UK) were trypsinised, pelleted and counted. 1×10^7 cells were prepared for injection into each animal. Cells were washed and centrifuged 3 times in and re-suspended in a volume of 250 μL for injection. On the 26^{th} post-operative day, cells were injected directly into the SIEA flap and monitored daily for tumour growth. Tumours were irradiated with 20 Gy in 5 consecutive, daily fractions when they reached a diameter of 1 cm.

Clinical outcomes

Skin paddle dimensions along the long (*x*) and short (*y*) axes of the skin paddle were quantified by caliper measurements between tattooed points. Skin paddle surface area was estimated using the formula: $area = 0.8*(xy)$. Early and late adverse effects were scored according to the Radiation Therapy Oncology Group (RTOG) adverse effects criteria(*49*).

In vivo MR imaging

For MRI, rats were anaesthetised with isoflurane and positioned within a 64 mm i.d. birdcage ^1H coil in a 7 Tesla horizontal bore microimaging system (Bruker Biospin, Ettlingen, Germany). Morphological multi-slice RARE fat-suppressed T_2-weighted axial images were first acquired for both localization of and subsequent determination of the flap volume. Contiguous 1mm thick images were acquired over a 6x6cm field of view (FOV), using a 128 by 128 matrix,

a repetition time (TR) of 4500ms, an echo time (TE) of 33ms, and 4 averages, giving an overall acquisition time of 4 minutes and 48 seconds. To quantify R_2*, multiple gradient echo (MGE) images were then acquired from three 1.56mm thick transverse slices through the pedicle, using 8 averages of 128 phase encoding steps over a 6×6cm field of view, giving a temporal resolution of 3.5 minutes. MGE images were acquired using a train of 8 echoes spaced 3.14ms apart, initial TE = 6.21ms, flip angle α = 45° and TR = 200ms. Tumour R_2* maps were calculated from the MGE images by fitting a single exponential to the signal intensity echo time curve on a voxel-by-voxel basis using a Bayesian maximum *a posteriori* approach(*73*). All post-hoc MRI processing and image reconstructions were performed using either OsiriX DICOM Viewer (OsiriX Foundation, Geneva, Switzerland) or in-house software (Imageview, developed in IDL, ITT Visual Information Systems, Boulder, CO, USA).

Functional vascular staining

Changes in vascular function were probed using a markers for perfused blood vessels (Hoechst 33342 (Sigma-Aldrich, Gillingham, UK)), vascular permeability (Evans Blue (Sigma-Aldrich, Gillingham, UK) and hypoxia (pimonidazole) (*74*) (Hypoxyprobe, Burlington, USA). At the experimental end point, animals were anaesthetized using inhalational isoflurane. Forty-five minutes prior to euthanasia, animals were administered Evans blue (i.v. 50mg/kg) and pimonidazole (i.p. 80mg/kg) and kept warm on a heated mat. Following this, Hoechst 33342 (i.v. 15mg/kg) was administered and a minute later euthanasia was performed. Flaps were harvested and frozen over liquid nitrogen. Non-consecutive 10μm sections were cut from frozen specimens and fixed in ice cold acetone for 10 minutes, covered in PBS and fluorescent imaging for Hoechst 33342 and Evans blue performed at 365nm and 520-550nm respectively using a motorized scanning stage (Prior Scientific Instruments, Cambridge, UK) and a BX51 microscope (Olympus Medical, Southend, UK). Images were acquired using CellP software (Soft Imaging System, Munster, Germany). The same slides were then washed in PBS and blocked in 200μL of an immunofluorescence (IFF) buffer for 1 hour at room temperature. Samples were incubated with a FITC-conjugated anti-pimonidazole primary antibody (1:200 in IFF) overnight at 4°C. The following day slides were washed in PBS and sections covered in PBS prior to pimonidazole imaging. Images were acquired at 450-499nm as described above using the same stage co-ordinates and, finally, the sections were stained with haematoxylin and eosin (H&E). Images of sections were acquired from 3 non-consecutive sections taken from each processed flap. The area of the section expressing Hoechst 33342, Evans blue and pimonidazole adduct fluorescence was quantified on whole section composite images and expressed as percentage of whole section (mean % section stained).

Lentiviral vectors

The LVSOD2 plasmid was created by Capital Biosciences (pLV_III_SOD2) (Capital Biosciences, MD, USA) for use *in vitro* and *in vivo* and control plasmids (LVeGFP) encoding acquired from the same source. Second-generation packaging plasmids were used for the production of all in-house viral particles (Addgene, Cambridge, MA, USA).

For CTGF knock down, the HIVSiren plasmid (kindly donated by Professor Greg Towers, University College London), constructed with either eGFP or puromycin-resistance

cassettes, was used. This plasmid is derived from a parent plasmid, CSGW (Prof Adrian Thrasher, University College London)(*75*).

CTGF knock down

The rat CTGF mRNA sequence (NCBI: NM_022266.2) was used to obtain knock down target sequences using an online RNAi target locator tool (http://www.clontech.com/GB/Support/xxclt_onlineToolsLoad.jsp?citemId=http://bioinfo.clontech.com/rnaidesigner/sirnaSequenceDesignInit.do&section=16260&xxheight=1100). The specificity of these sequences were checked by cross referencing them against known rat genomic DNA sequences and a non-silencing, scrambled RNAi sequences was also generated Hairpins were designed to include *BamHI* (GGATCC) and *EcoRI* (GAATTC) overhangs at the 5' and 3' ends, respectively, as well as the *MluI* restriction site (ACGCGT) within the hairpin sequence itself.

Generation ofp LVshCTGF and pLVshSCRAM

Oligonucleotides encoding the shRNA sequences were annealed by adding 2.5 μL 2 M sodium chloride solution to 10 μL of each oligonucleotide. The mix was heated for 5 minutes at 98°C and then slowly cooled at 0.1°C per second until 4 °C before adding 350 μL RNase-free water, 40 μL 3 M sodium acetate, 1.1 mL absolute ethanol and incubated at -80°C overnight. The following day the annealed oligonucleotides were thawed and spun in a table-top centrifuge at 13,000 rpm, for 45 minutes at 4°C. The supernatant was then aspirated and the pellet air-dried before reconstitution in 50 μL RNase-free water.

A double restriction digest was performed on the HIVSiren backbone using *BamHI* and *EcoRI* (New England Biolabs, Hitchin, UK). In brief, 5 μg of HIVSiren plasmid DNA was digested with 10 units of BamHI (2 μL), 10 units of EcoRI (2 μL), 5 μL EcoRI buffer and 0.5 μL 10X bovine serum albumin (BSA) made up to a total volume of 50 μL. The reaction was then incubated in a water bath at 37°C for 90 minutes. Following this, 10 μL of X6 bromophenol blue gel-loading dye was added to the reaction and gel electrophoresis performed using a 1% agarose gel (in 100 mL Tris/Acetic acid/EDTA buffer + 20 μL ethidium bromide). Electrophoresis was performed at 100 V for 45 minutes and DNA bands were visualized using a 302 nm ultraviolet transilluminator. Bands that demonstrated a linearization event were excised and DNA extracted from these using a commercially-available DNA extraction kit for subsequent ligation reactions.

Ligation reactions were performed using: 120 ng of vector DNA, annealed oligonucleotide insert DNA (at a 1:3 and 1:5 molar ratio), 0.2 μL DNA T4 ligase (ThermoScientific, Fischer Scientific UK Ltd., Loughborough, UK), 2 μL ligase buffer and diethylpyrocarbonate-treated (DEPC-treated) water (ThermoScientific, Fischer Scientific UK Ltd., Loughborough, UK) to a total volume of 20 μL. Ligations were carried out for 15 minutes at room temperature alongside negative controls consisting of vector DNA only. Ligation reactions (5 μL) were used to transform DH5-α™ competent cells (50 μL) (Invitrogen, Life Technologies Ltd., Paisley, UK) using a heat-shock method. Following this, organisms were

recovered by the addition of 200 μL of SOC medium (2% tryptone, 0.5% yeast extract, 10 mM NaCl, 2.5 mM KCl, 10 mM $MgCl_2$, 10 mM $MgSO_4$, and 20 mM glucose) (Invitrogen, Life Technologies Ltd., Paisley, UK) and plated at serial dilutions (1:10-1:1000) on ampicillin (50 mg/mL) L-agar plates overnight. The next day single colonies were picked from each plate and used to inoculate a starter culture of 5 mL Terrific broth (+100 μg/mL ampicillin (Sigma-Aldrich, Gillingham, UK); CSSD, ICR, Chelsea, London). This was incubated at 37ºC and shaken at 220 rpm overnight, following which bacteria were pelleted and DNA extracted using the Qiaprep© Spin Miniprep kit (Qiagen Ltd., Manchester, UK).DNA was sent for sequencing using a primer-based protocol (sequencing primer: 5' ATGCCAATTGCTCCTTCTCTAGGCGCCGGAAT 3'). Sequences were analysed using Sequencher 4.8 (Ann Arbor, MI, USA) and cross-checked against hairpin sequences to ensure the correct sequence and orientation before using the DNA for lentivirus production.

Generation of LVshCTGF and LVshSCRAM

HEK 293T cells (4×10^6) were plated in a tissue culture dish and transfections performed the following day if cells were greater than 80% confluent.

Transfections were performed using the Lipofectamine® 2000 protocol using lentiviral backbone plasmids (pLVshCTGF, pLVSCRAM, pLV_III_SOD2) (CBS) (Capital Biosciences Ltd, Rockville, MD, USA) and 2nd generation packaging co-plasmids (psPAX2 and pMD2.g (Addgene, Cambridge, MA, USA). A Lipofectamine®/Opti-MEM® (Life Technologies, Paisley, UK) mix was made and combined with a DNA/Opti-MEM® mix and allowed to incubate at room temperature for 5 minutes. The medium from the HEK 293T cells was removed and replaced with fresh medium and the Lipofectamine®/DNA/Opti-MEM® mixture was added to the plate drop-wise. The plate was incubated at 37°C overnight in an incubator (95% air and 5% CO_2) and the following morning the transfection medium was removed and replaced with collection medium (OptiMEM® + 1:20 cholesterol + 2 mM l-arginine and 1% penicillin/streptomycin). Supernatant containing viral particles was harvested up to 72 hours after this time and filtered through a 0.45 μm filter (Life Technologies, Paisley, UK).

Viral particles were concentrated using an ultracentrifugation method (UCF) with a sucrose cushion. UCF tubes (Thinwall, Ultra-Clear™, 38.5 mL, 25 x 89 mm; Beckman, High Wycombe, UK) were part filled with viral supernatant and a 25% sucrose solution (25.4 g of sucrose (Sigma-Aldrich, Gillingham, UK) to a volume of 100 mL with sodium phosphate buffer (50 mM, pH 7.4) and filter-sterilized) was pipetted into the tube as an underlay. Centrifugation was performed at 23,000 rotations per minute (rpm) for 2 hours at 4°C in a vacuum. The pellet was re-suspended in 1 mL PBS.

Lentiviral titres were quantified using a functional, GFP expression assay following the infection of target cells. On day 1, 1×10^5 HeLa cells/well were plated on a 24-well plate in DMEM (5% FCS + 2 mM l-arginine + 1% penicillin/streptomycin). The following day inoculation was performed using serial dilutions (1:100-1:10,000) of viral supernatant (400 μL) (+ 1 μg/mL polybrene). Cell counts were also performed across 3 wells and averaged to give a target cell population at the time of infection. The next day the inocula were aspirated and the wells replenished with fresh medium. On day 5, the cells were trypsinised and re-suspended in a

2 mL of medium for fluorescence-activated cell sorting (FACS) using the BD LSR II FACS machine (BD Biosciences, Oxford, UK). A threshold of 3-fold above background signal was used to gate for GFP positive cells. Following quantification of GFP expression, the titre (in transducing units per mL) was calculated using the following formula: Titre (TUs / mL) = [(% GFP^+ cells/100) x (no. cells per well/volume inoculum)] x dilution. The final titre was calculated as the average of triplicate assays.

Supplementary Materials

Fig. S1. Development and validation of a novel model of free flap LAEs.

Fig. S2. Validation of CTGF knock down using LVshCTGF.

Materials and Methods

Acknowledgments: We would like to thank the following people for assistance in carrying out this work: Dr F Daley, Dr A McCarthy, Dr D Roberts, Ms C Gregory, Dr A Fletcher, Dr L Baker, Dr H Barker. **Funding:** AAK and JTP were funded by The Wellcome Trust (WT098937MF and 200175/Z/15), The Royal College of Surgeons of England, BAPRAS and the Masons Medical Research Foundation. VR, JNK and KJH were funded by the ICR/RMH NIHR Biomedical Research Centre and the Rosetrees Trust. KJH also received funding from the Oracle Cancer Trust and the Anthony Long Trust. SPR acknowledges the support received for The Institute of Cancer Research Cancer Research UK and EPSRC Cancer Imaging Centre (grant C1060/A10334) and to the Cancer Research Cancer Imaging Centre (C1090/A16464) in association with the MRC and Department of Health (England). MH was funded by the Cancer Research Funds of Radiumhemmet, the Stockholm County Council and the Swedish Society of Medicine. **Author contributions:** AAK, KH and PAH contributed to the conceptualization and study design. AAK, MM, JP, JK, MW, TP, DM and VR designed and executed *in vitro* studies. AAK, RS, JP and TP executed *in vivo* surgical studies. JB and SR performed imaging analyses. AAK and MH performed data analyses. AAK and KH wrote the manuscript. NS, HP, RV, AM and PAH performed critical review of the data and oversight. **Competing interests:** None declared. **Data and materials availability:** Materials can be obtained from the ICR via a material transfer agreement.

Figures:

Fig. 1. Irradiation with 50 Gy/3 fractions generates a LAE phenotype characterized by SOD2 depletion and CTGF over-expression.

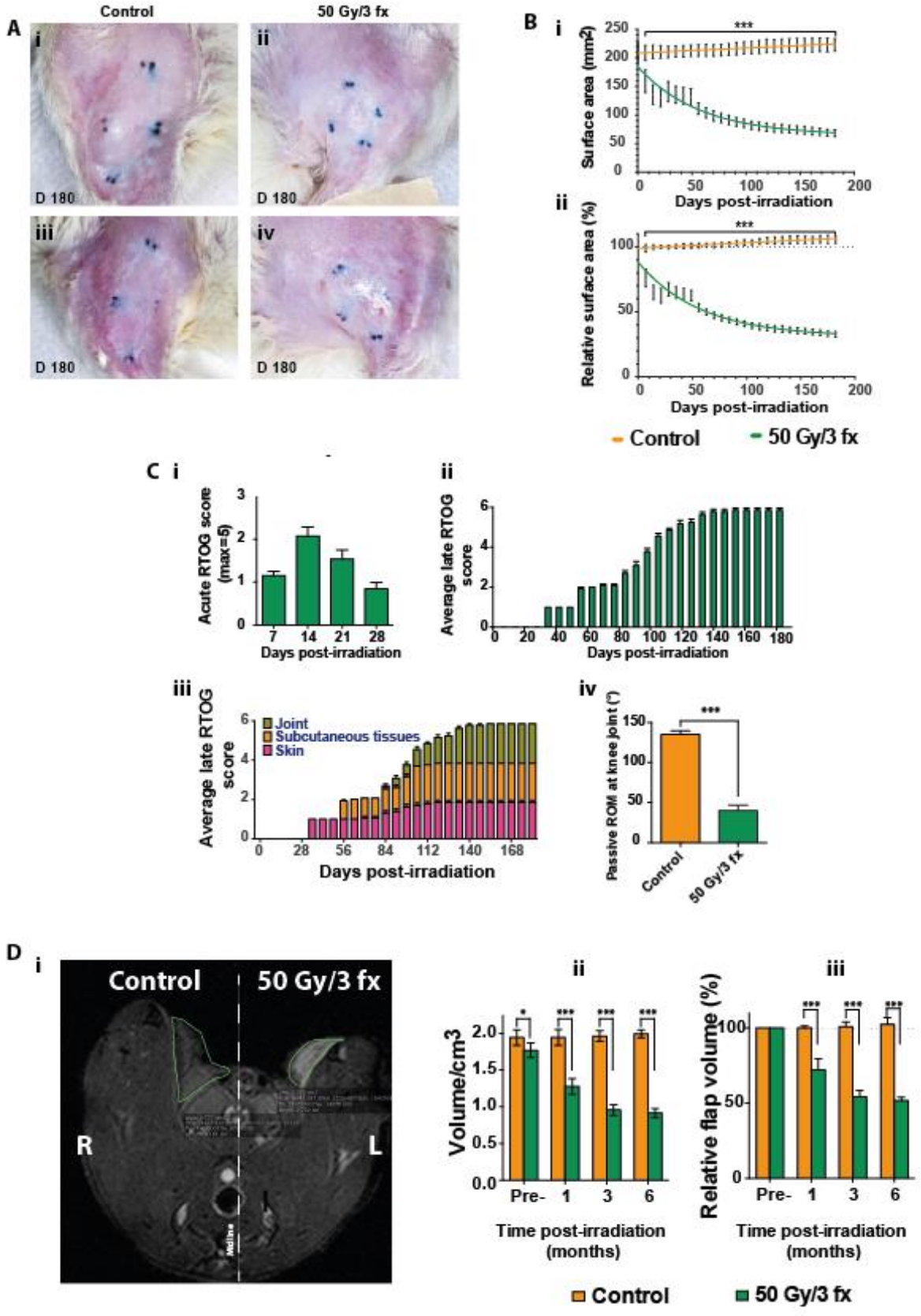

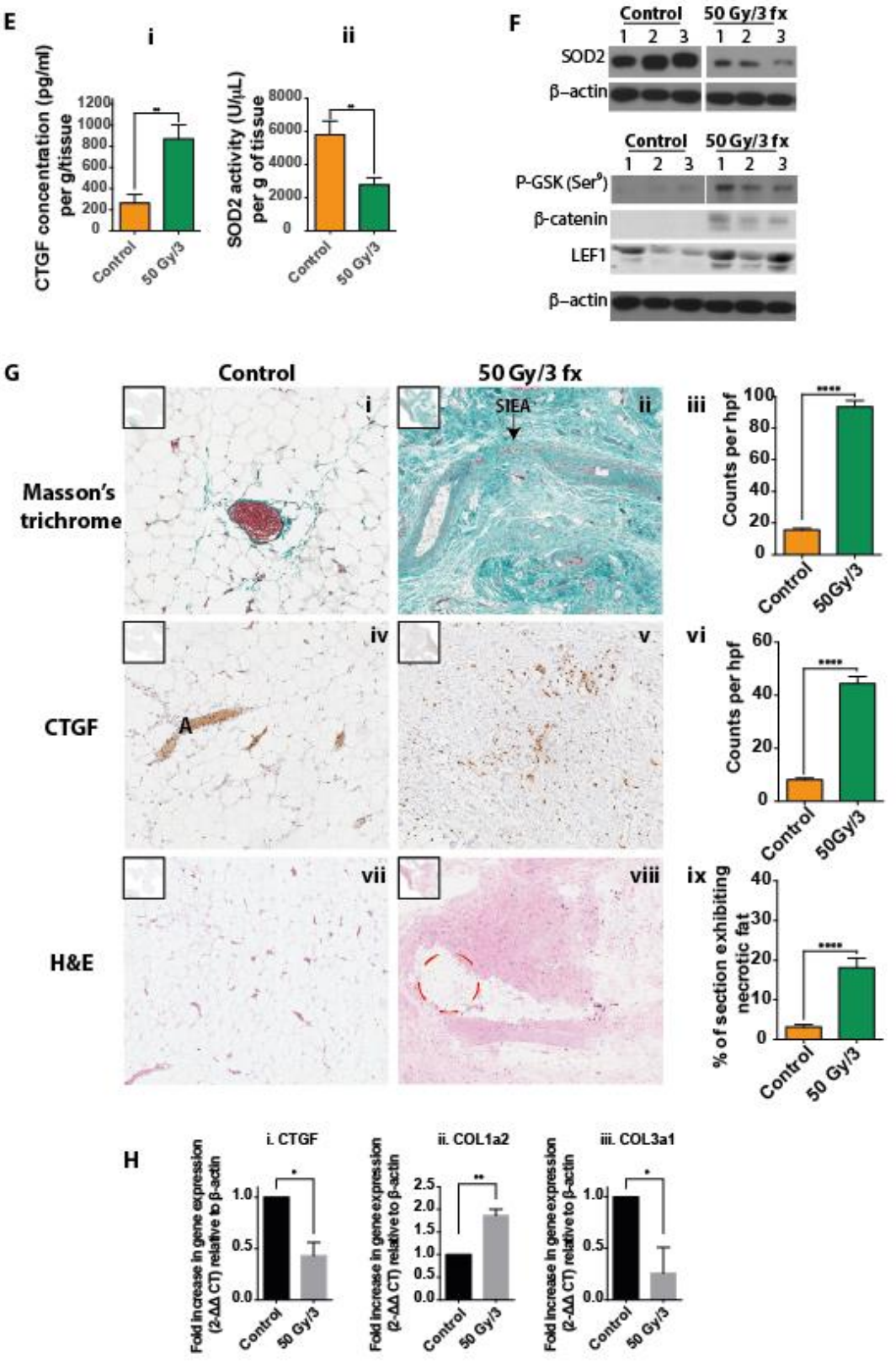
E
i
ii
CTGF concentration (pg/ml) per g/tissue
SOD2 activity (U/μL) per g of tissue
Control
50 Gy/3
F
Control
50 Gy/3 fx
1 2 3 1 2 3
SOD2
β–actin
P-GSK (Ser9)
β-catenin
LEF1
G
Control
50 Gy/3 fx
Masson's trichrome
CTGF
H&E
SIEA
A
Counts per hpf
% of section exhibiting necrotic fat
H
i. CTGF
ii. COL1a2
iii. COL3a1
Fold increase in gene expression (2-ΔΔ CT) relative to β-actin

Figure 1. Irradiation with 50 Gy/3 fractions generates a LAE phenotype characterized by SOD2 depletion and CTGF over-expression. A) Representative photographs of bilateral SIEA flaps (edges tattooed in Indian ink) inset onto the hind limbs of Fischer (F344) male rats taken at 180 days after irradiation. The left limb flaps (ii and iv) were irradiated with 50 Gy/3 fractions on consecutive days whereas flaps on the contralateral limb did not undergo irradiation. Flap skin paddles were not significantly different prior to irradiation. Characteristic LAE features were observed in irradiated flaps including contracture, induration of the skin, telangiectasia and hair loss (un-irradiated flaps have been shaved to expose marked edges, whereas irradiated flaps have not) (supplementary figure 1). **B)** Changes in skin paddle surface area of irradiated and control SIEA flaps demonstrating significant losses in absolute (i) and relative (ii) skin paddle surface area (± 95% CI). Irradiated flaps were observed to lose up to 70% of their pre-irradiation skin paddle surface area ($p<0.0001$). **C)** Acute and late RTOG scores. i) Acute RTOG scores (mean ± SEM) demonstrating the duration and severity of acute toxicities observed in flaps irradiated with 50 Gy/3 fx. ii) Late RTOG scores (mean ± SEM) in flaps irradiated with 50 Gy/3 fx demonstrating progressive severity of LAEs in irradiated flaps. iii) Component scores for the RTOG late effects scores demonstrating that LAEs were first evident in the skin followed by the subcutaneous tissues and joint. iv) Passive ROM at the knee joint in irradiated and non-irradiated hind limbs demonstrating a significant reduction in knee joint excursion in irradiated hind limbs compared to controls. [*** $p < 0.0001$]. **D)** i) T_2-weighted MR image of bilateral SIEA flaps showing an irradiated flap (left) and un-irradiated control (right) at 180 days after irradiation (flaps outlined in green). Note the apparent shrinkage in flap cross-sectional area in the irradiated flap compared to control. ii) Mean MRI-derived absolute flap volume (± 95% CI) showing significant flap volume loss in irradiated flaps. iii) Relative MRI-derived flap volume changes (normalized to pre-irradiation volumes) (± 95% CI) demonstrating that irradiated flaps lose up to 50% of their pre-irradiation volume by 6 months. [* $p < 0.05$, *** $p < 0.0001$]. **E)** i) CTGF ELISA on flap tissues taken from both irradiated and control flaps (180 days post-RT) demonstrating an increase in CTGF protein concentration in irradiated flaps. ii) SOD2 activity measurement by biochemical assay demonstrating a significant reduction in SOD2 activity in irradiated flaps (52% decrease) compared to controls. [** $p < 0.01$]. **F)** Western blotting of matched control and irradiated SIEA flaps (at 180 days post-RT) showing reductions in SOD2 protein expression (upper panel) and activation of Wnt-signalling through phosphorylation of GSK-3β. **G)** Immunohistochemical analysis of irradiated flaps (180 days post-RT) with Masson's trichrome (i-iii), CTGF (iv-vi) and fat necrosis (vii-ix) demonstrating significant increases in collagen deposition (i and ii; green staining), CTGF (iv and v) and fat necrosis (vii and viii; red dashed circle). Graphs represent mean ± SEM of counts per high powere field (hpf) or % section exhibiting fat necrosis. **H)** RT-QPCR for *CTGF*, *Col1a2* and *Col3a1* gene expression (mean fold increase in gene expression ± SEM) (flaps harvested at 180 days post-RT) demonstrating significant reductions in *CTGF* and *Col3a1* expression but significant increases in *Col1a2* gene expression [*$p<0.05$, **$p<0.01$, **** $p < 0.0001$].

Fig. S1. Development and validation of a novel model of free flap LAEs

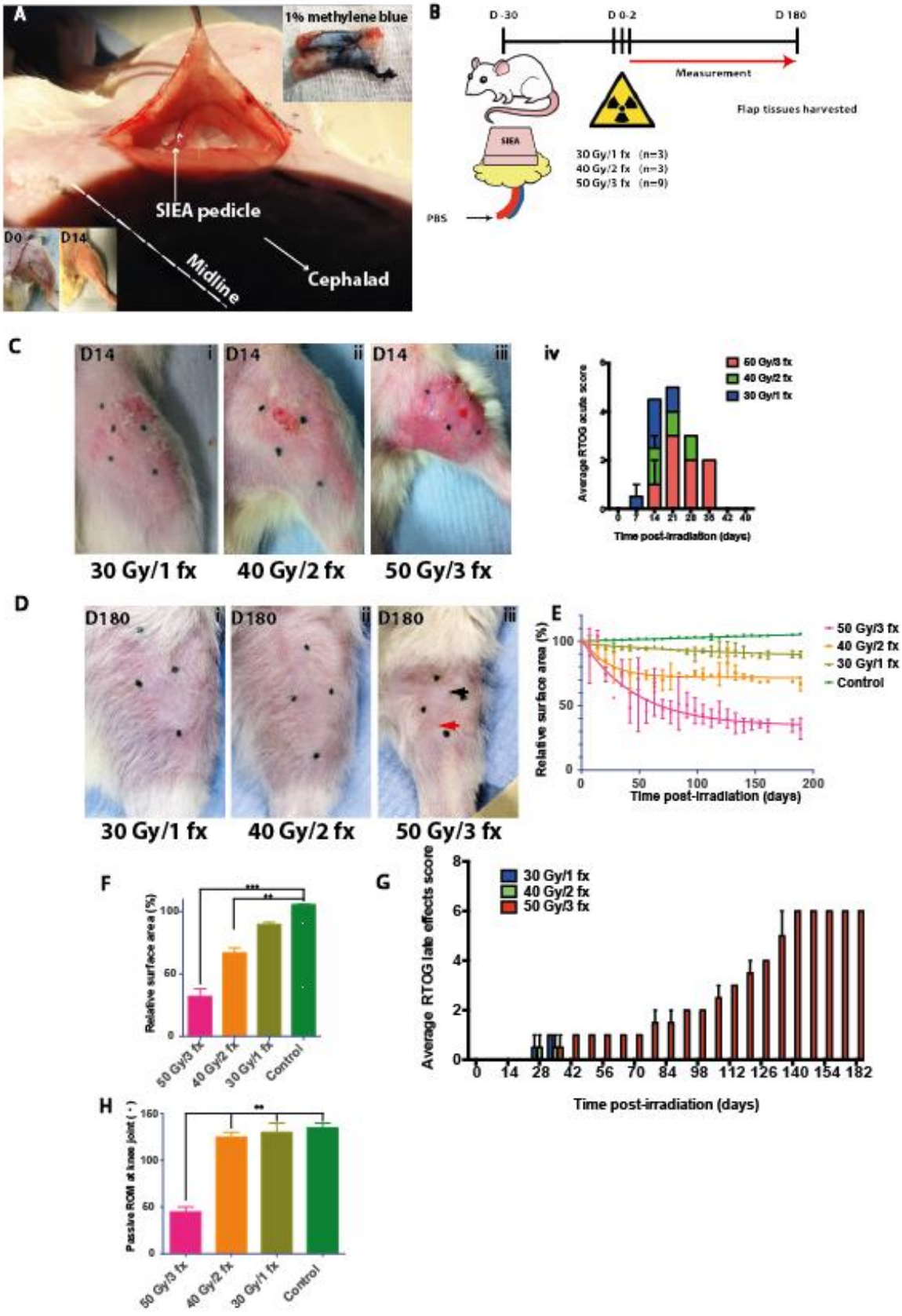

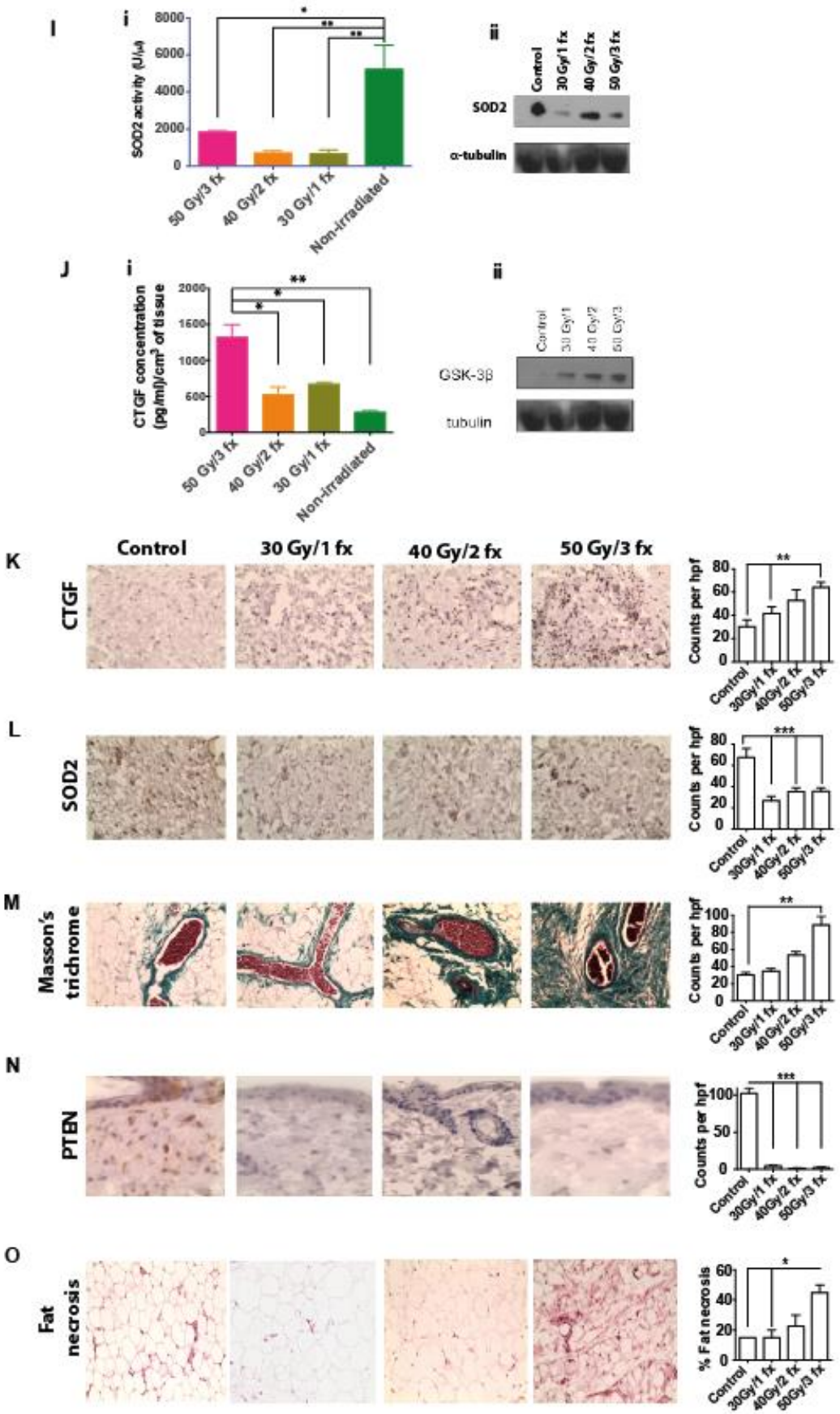
I
i
SOD2 activity (U/μl)
8000
6000
4000
2000
0
*
**
**
50 Gy/3 fx
40 Gy/2 fx
30 Gy/1 fx
Non-irradiated
ii
Control
30 Gy/1 fx
40 Gy/2 fx
50 Gy/3 fx
SOD2
α-tubulin
J
i
CTGF concentration (pg/ml)/cm³ of tissue
2000
1500
1000
500
0
**
*
*
50 Gy/3 fx
40 Gy/2 fx
30 Gy/1 fx
Non-irradiated
ii
Control
30 Gy/1
40 Gy/2
50 Gy/3
GSK-3β
tubulin
K
Control
30 Gy/1 fx
40 Gy/2 fx
50 Gy/3 fx
CTGF
Counts per hpf
80
60
40
20
0
**
Control
30Gy/1 fx
40Gy/2 fx
50Gy/3 fx
L
SOD2
Counts per hpf
80
60
40
20
0
***
Control
30Gy/1 fx
40Gy/2 fx
50Gy/3 fx
M
Masson's trichrome
Counts per hpf
100
80
60
40
20
0
**
Control
30Gy/1 fx
40Gy/2 fx
50Gy/3 fx
N
PTEN
Counts per hpf
100
50
0
***
Control
30Gy/1 fx
40Gy/2 fx
50Gy/3 fx
O
Fat necrosis
% Fat necrosis
60
40
20
0
*
Control
30Gy/1 fx
40Gy/2 fx
50Gy/3 fx

744

745

Fig. S1. Development and validation of a novel model of free flap LAEs. A) The surgical superior inferior epigastric artery (SIEA) flap model. Main photograph shows the SIEA flap being raised from the lower abdomen and the SIEA pedicle entering flap tissues and bifurcating. The SIEA can be cannulated and infused with as shown in the photograph (top right) where 0.5 mL of a 1% methylene blue solution has been infused. Flaps are inset into the ventral hind limb and the donor site closed primarily with wound healing being complete by 2 weeks post-operatively (bottom left). **B)** Schematic of the fractionation pilot study comparing 3 biologically equivalent fractionation regimens (n=3 per cohort): 30 Gy/single fraction, 40 Gy/2 fractions or 50 Gy/3 fractions. Fractions were all delivered on consecutive days. SIEA flaps were inset into the hind limb and were irradiated 30 days post-operatively. Animals were maintained for 180 days with clinical and radiological follow-up prior to flap tissues being harvested for histological and molecular analyses. **C)** Representative photographs (dots represent SIEA flap margins) demonstrating the spectrum of acute toxicities observed following irradiation: i) dry desquamation, ii) patchy moist desquamation and iii) confluent wet desquamation. Acute toxicities can be quantified using the RadioTherapy Oncology Group (RTOG) acute scoring system (iv), which demonstrated that flaps irradiated with 50 Gy/3 fractions exhibited the most sustained acute toxicities. Flaps irradiated with 30 Gy and 40 Gy fractionation regimens developed acute toxicities for a shorter duration (21 days). **D)** Appearance of SIEA flaps at 180 days post-irradiation showing that flaps irradiated with 50 Gy/3 fractions exhibit a phenotype that is characteristic of LAEs as demonstrated by the presence of significant contracture, pigmentation change (black arrow), telangiectasia (red arrow) and hair loss. **E** and **F**) Quantification of skin paddle surface area (mean ± 95% CI) showed that contracture was seen in all 3 fractionation cohorts but the greatest degree of contracture was observed in the 50 Gy/3 fraction cohort. **G)** RTOG late adverse effect scoring demonstrated that only the 50 Gy/3 fraction cohort developed measureable LAEs that became progressively more severe over the duration of the experiment. These changes were observed both in cutaneous, subcutaneous and underlying joint tissues. **H)** LAEs affecting knee joint function and passive range of movement (ROM) developed late in the experiment in the 50 Gy/3 fraction cohort whereas animals with SIEA flaps irradiated with 30 and 40 Gy did not develop any LAEs in their joints. **I)** SOD2 biochemical assay (i) demonstrating significant reductions in SOD2 activity in irradiated flaps compared to control flaps even at 180 days post-irradiation. SOD2 activities between fractionation cohorts were not significantly different however a trend was observed to suggest that the greatest reductions were observed with the largest doses per fraction. ii) Western blot for SOD2 demonstrating a similar pattern of reduction in protein expression levels in irradiated flaps compared to controls. **J)** i) ELISA for CTGF demonstrating significant increases in CTGF expression in irradiated flap tissues harvested at 180 days post-irradiation. The 50 Gy/3 fraction cohort exhibited the greatest increases in CTGF concentration. Western blot analyses for phosphorylated GSK-3β (Ser^9) demonstrating increases in GSK-3β phosphorylation with total radiation dose delivered (image representative of all experiments) suggesting activation of the Wnt-pathway following irradiation. K-O) Histological analysis of irradiated SIEA flaps. **K)** Immunohistochemical staining for CTGF demonstrating a significant increase in CTGF expression in flaps irradiated with 50 Gy/3 fx compared to controls and those irradiated with 30 Gy. **L)** SOD2 immunohistochemistry in irradiated and non-irradiated controls. The latter group exhibited significantly greater SOD2 expression compared to all irradiated groups. **M)** Masson's trichrome staining for collagen deposition in controls and irradiated flaps demonstrating a signficant increase in collagen deposition in flaps

irradiated with 50 Gy/3 fx. **N)** Dermal PTEN immunohistochemistry demonstrating a significant reduction in PTEN expression in all irradiated flaps. **O)** H&E staining for the quantification of fat necrosis within irradiated flaps demonstrating a significant increase in fat necrosis in flaps irradiated with 50 Gy/3 fx compared to controls and those irradiated with 30 Gy ($p = 0.039$). [*** $p < 0.0001$, ** $p < 0.01$, * $p < 0.05$].

Fig. 2. LAEs are characterized by vascular dysfunction, loss of endothelial perfusion and permeability and peri-vascular hypoxia

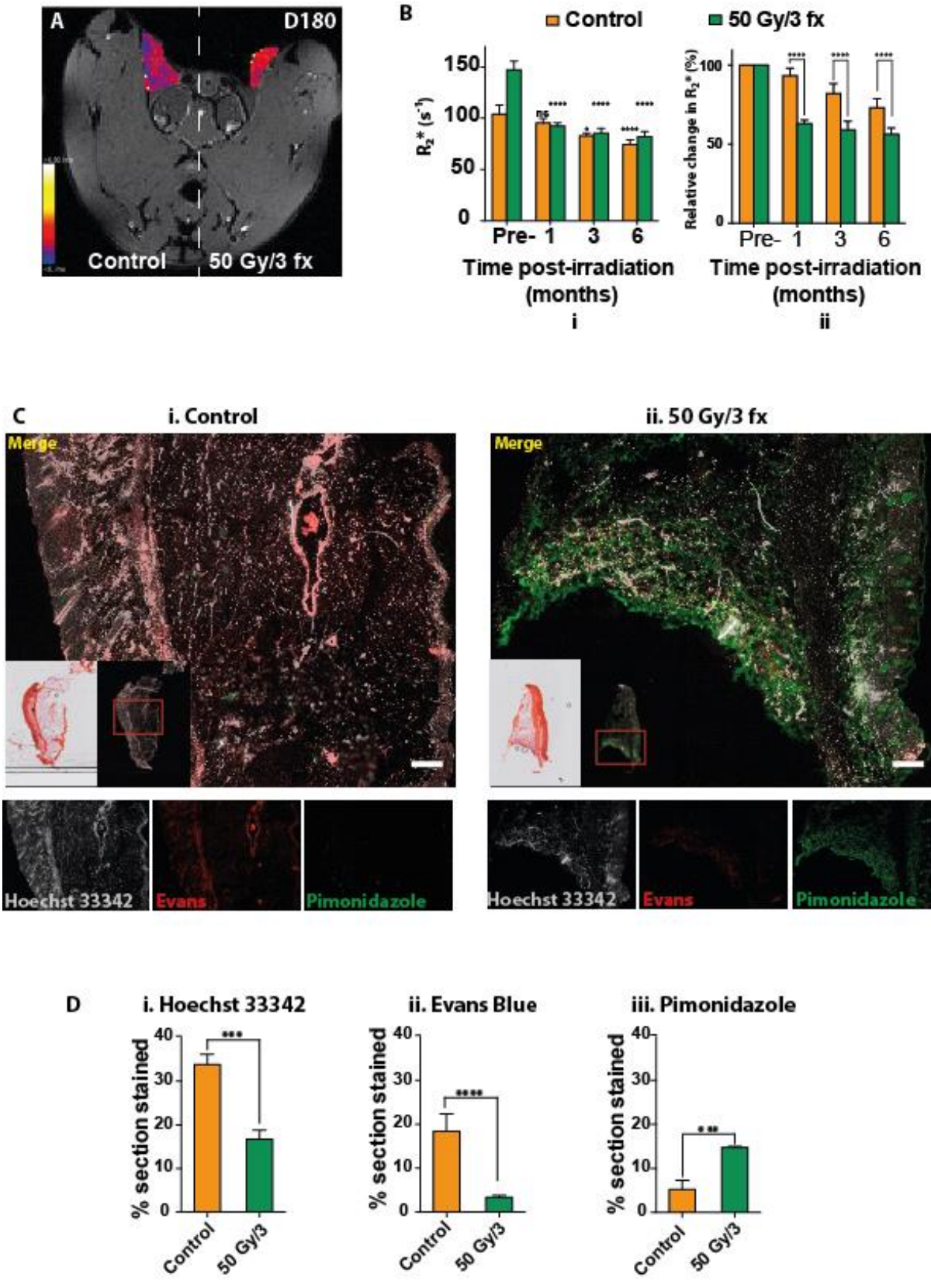

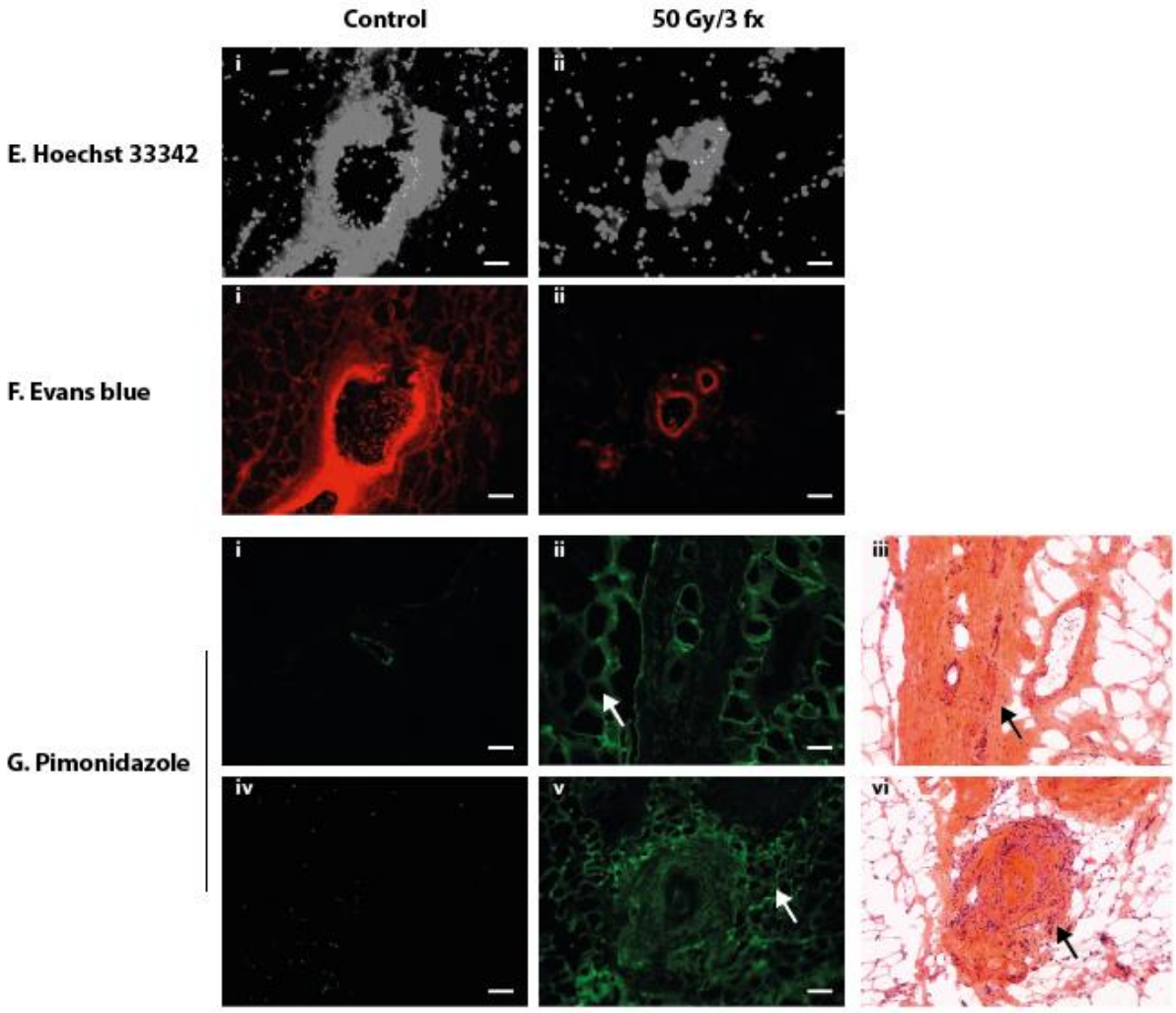

Figure 2. LAEs are characterized by vascular dysfunction, loss of endothelial perfusion and permeability and peri-vascular hypoxia. A) Parametric R_2* maps of control and irradiated flaps overlaid on T_2-weighted images acquired 6 months following irradiation. **B)** i) Absolute changes in R_2* (mean ± 1 SEM) demonstrating that, in irradiated flaps, basal R_2* was reduced significantly from 1 month onwards. Asterisks represent comparisons made with the pre-irradiation time point for each group separately. ii) Relative changes in R_2* (mean ± 1 SEM) demonstrating that irradiated flaps exhibited greater reductions in relative R_2* compared to control flaps at all post-irradiation time points. [ns = not significant, * $p < 0.05$, **** $p < 0.0001$]. **C)** Hoechst 33342 uptake, Evans blue leakage and pimonidazole adduct formation in control (i) and irradiated (ii) flaps (H&E and composite scan (x 10 magnification) of entire section inset with red box representing zoomed micrograph) demonstrating a significant reduction in Hoechst 33342 and Evans blue fluorescence and an increase in pimonidazole adduct immunofluorescence. **D)** Quantification of Hoechst 33342 uptake, Evans blue leakage and pimonidazole adduct formation. Bars represent mean percentage of section exhibiting staining (±SEM). Images are representative of the larger cohort (n = 3 animals with

bilateral flaps). Scale bars (bottom right) represent 100 μm. [*** $p < 0.001$, **** $p < 0.0001$]. **E, F** and **G)** Post-radiation changes in microvascular function demonstrating reductions in Hoechst 33342 uptake **(E)**, Evans blue fluorescence **(F)** and an increase in pimonidazole adduct immunofluorescence **(G)** (with H&E of section inset) in control and irradiated flaps with 50 Gy/3 fx. Note perivascular fibrosis around irradiated vessels (**G**.iii and vi; black arrow) and correlation with pimonidazole staining (**G**.ii and v; white arrow). Images are representative of the larger cohort. Scale bar (bottom right) is equal to 20 μm.

Fig. 3. Mitochondrial SOD2 over-expression in normal, but not tumour cells, mediates radioprotection across a range of fractionation schedules and durable *SOD2* over-expression can be achieved *in vivo*.

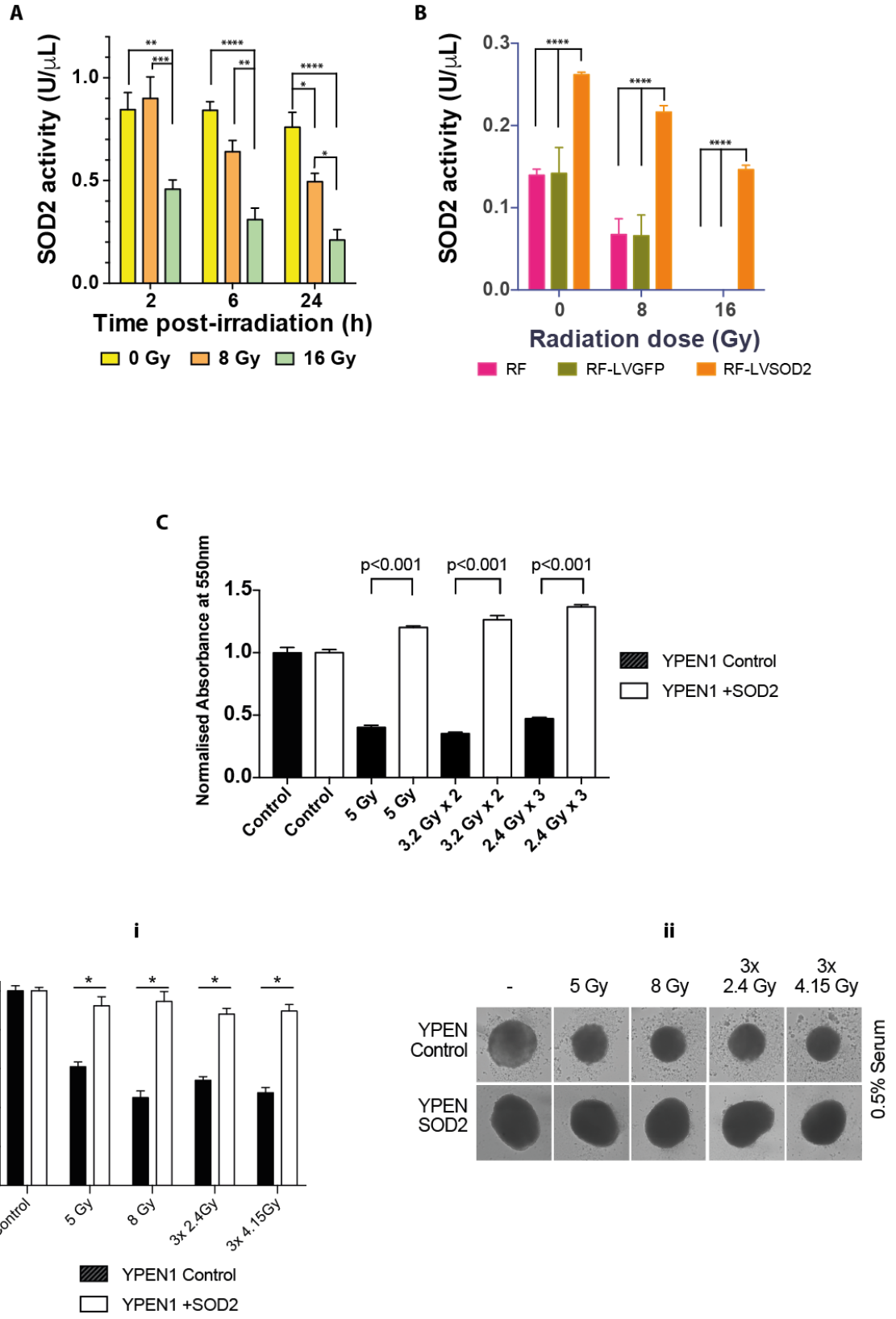

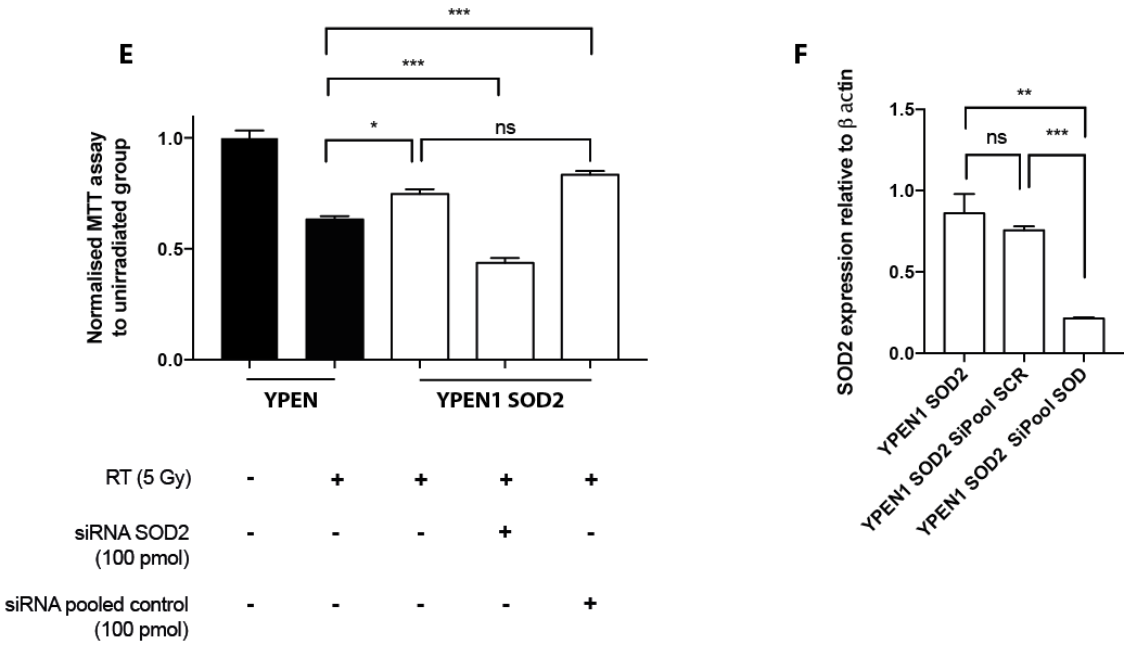
E
***
***
*
ns
Normalised MTT assay to unirradiated group
1.0
0.5
0.0
YPEN
YPEN1 SOD2
RT (5 Gy) - + + + +
siRNA SOD2 (100 pmol) - - - + -
siRNA pooled control (100 pmol) - - - - +
F
**
ns
***
SOD2 expression relative to β actin
1.5
1.0
0.5
0.0
YPEN1 SOD2
YPEN1 SOD2 SiPool SCR
YPEN1 SOD2 SiPool SOD

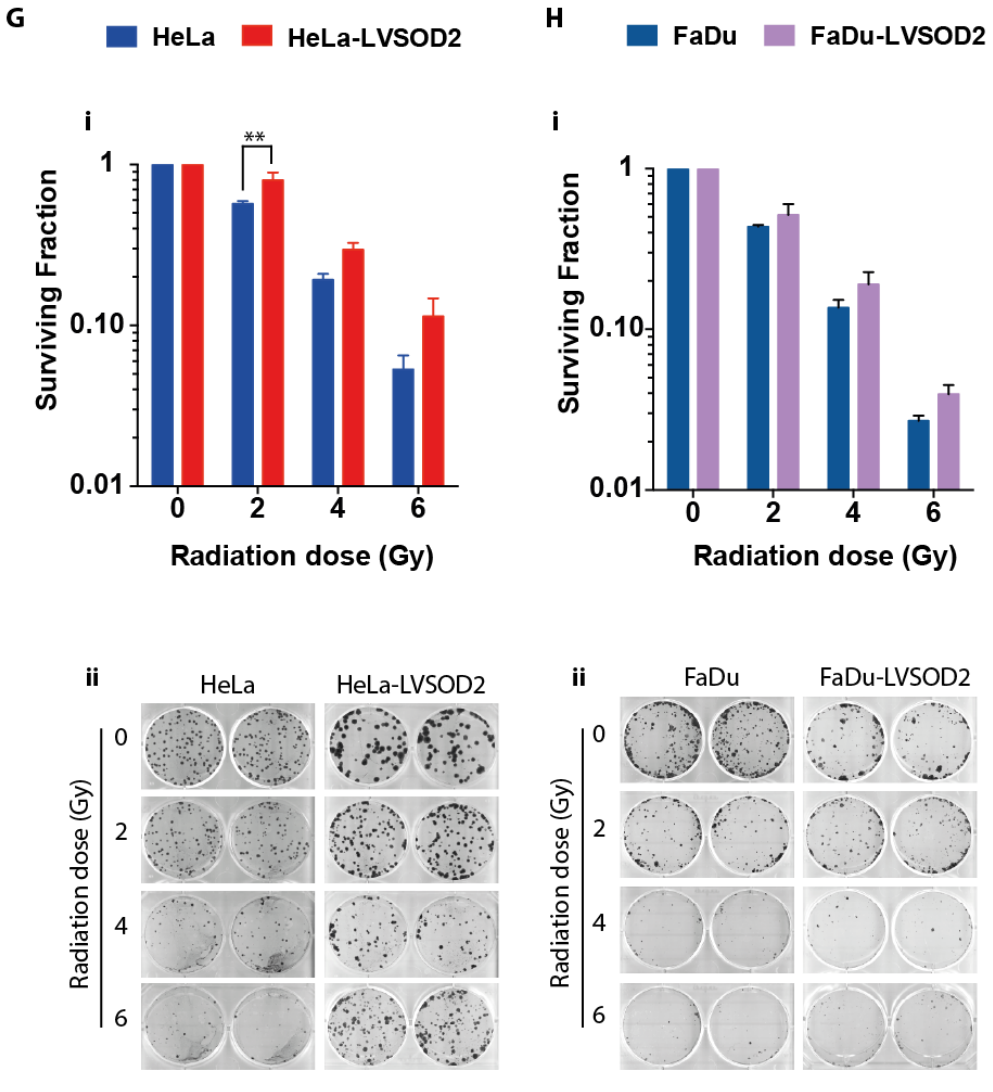
G
HeLa
HeLa-LVSOD2
i
**
Surviving Fraction
1
0.10
0.01
0
2
4
6
Radiation dose (Gy)
ii
HeLa
HeLa-LVSOD2
Radiation dose (Gy)
0
2
4
6
H
FaDu
FaDu-LVSOD2
i
Surviving Fraction
1
0.10
0.01
0
2
4
6
Radiation dose (Gy)
ii
FaDu
FaDu-LVSOD2
Radiation dose (Gy)
0
2
4
6

I

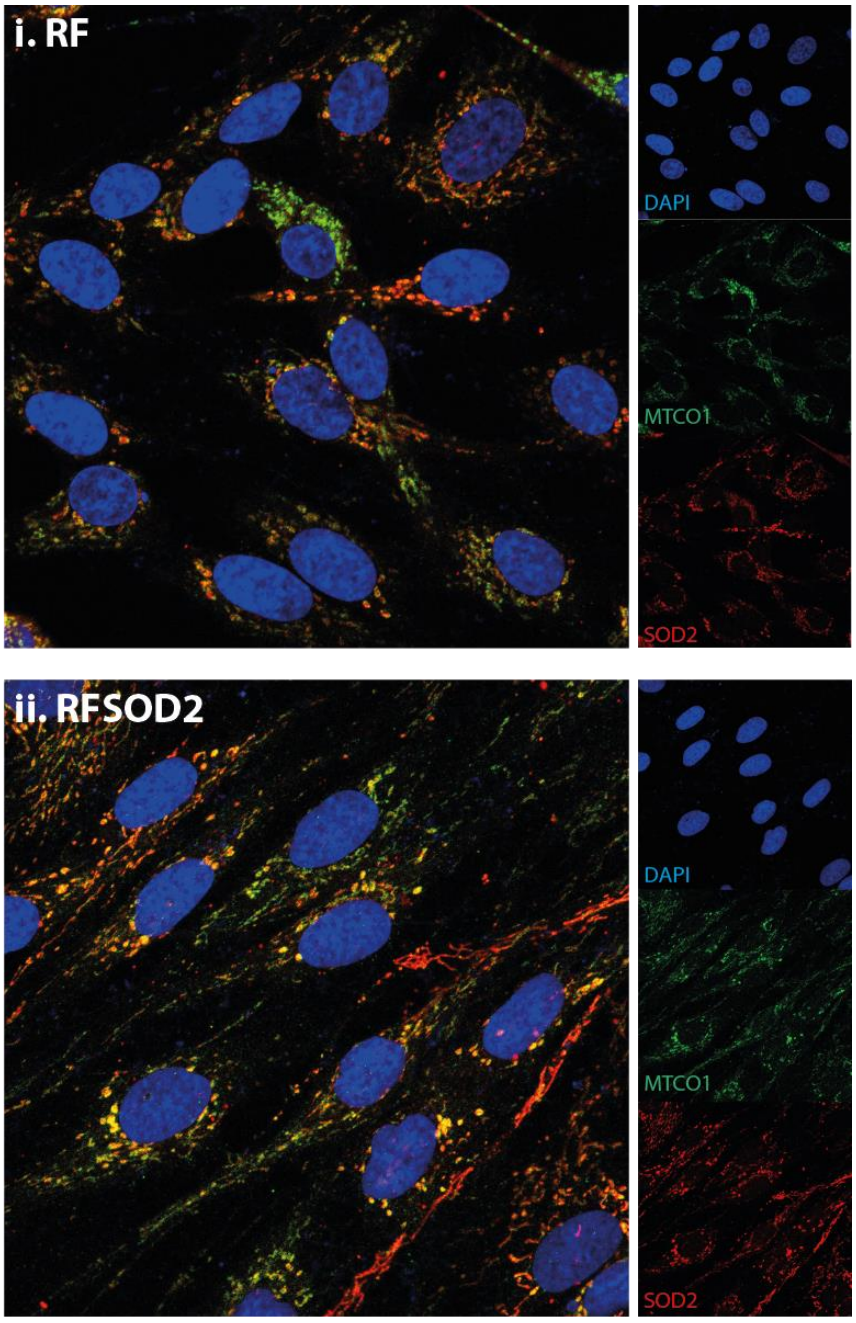
i. RF
DAPI
MTCO1
SOD2
ii. RFSOD2
DAPI
MTCO1
SOD2

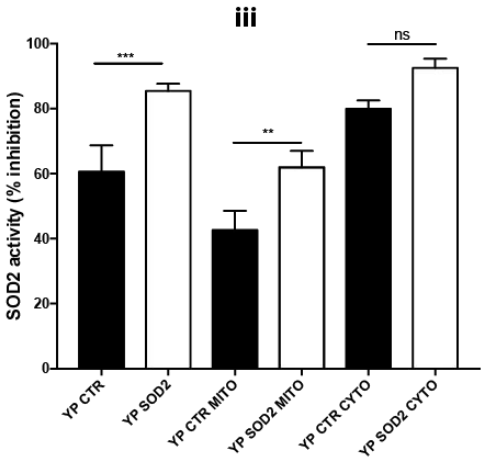
iii
SOD2 activity (% inhibition)
100
80
60
40
20
0
***
**
ns
YP CTR
YP SOD2
YP CTR MITO
YP SOD2 MITO
YP CTR CYTO
YP SOD2 CYTO

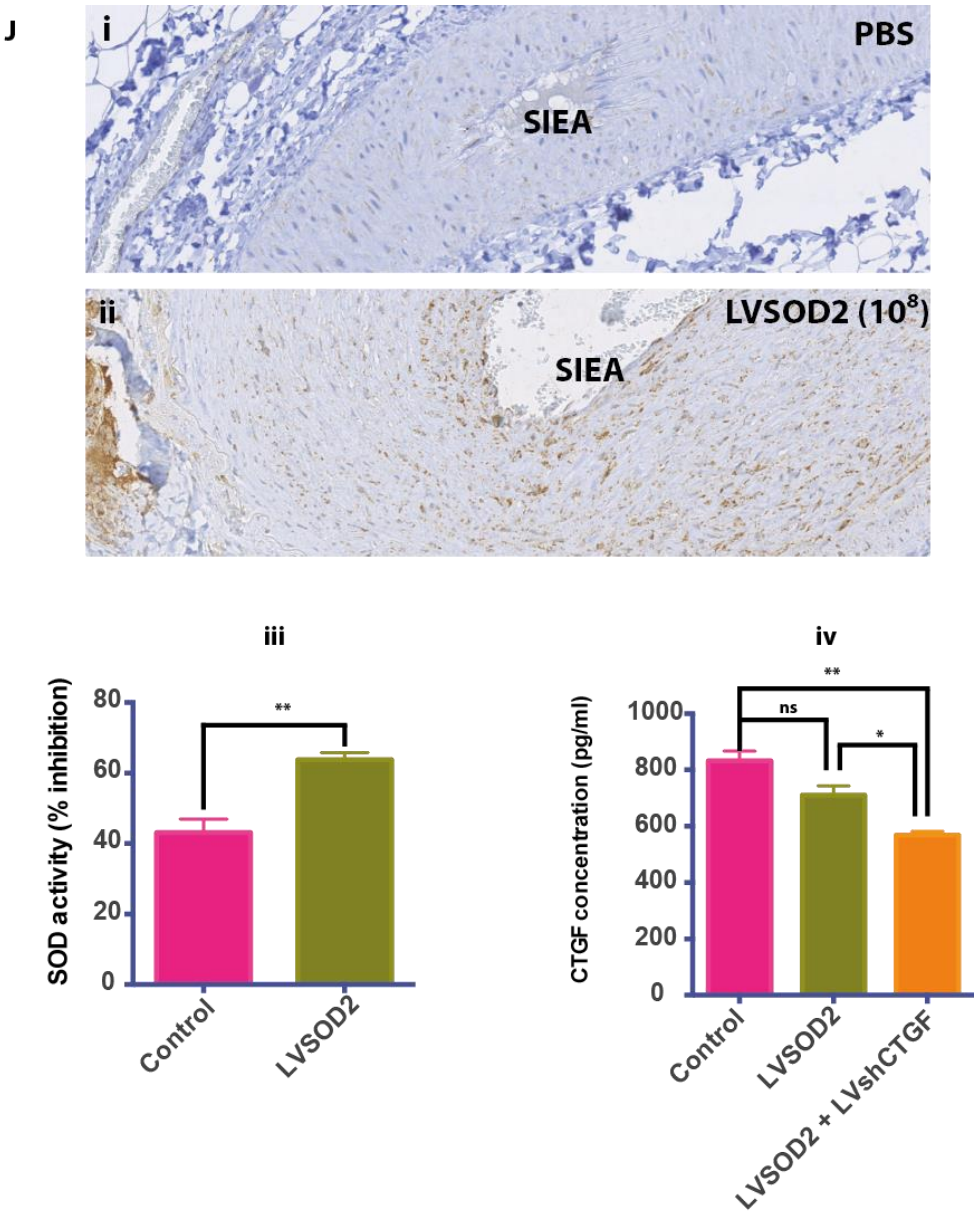
J
i
PBS
SIEA
ii
LVSOD2 (10^8)
SIEA
iii
SOD activity (% inhibition)
80
60
40
20
0
**
Control
LVSOD2
iv
CTGF concentration (pg/ml)
1000
800
600
400
200
0
**
ns
*
Control
LVSOD2
LVSOD2 + LVshCTGF
K
Fold change of SOD2 mRNA Expression compared to paired controls
2.0
1.5
1.0
0.5
0.0
*
PBS (sham)
LVSOD2 (10^8)
L
SOD2 activity (% inhibition)
100
90
50
40
30
20
10
0
*
PBS (sham)
LVSOD2 (10^8)

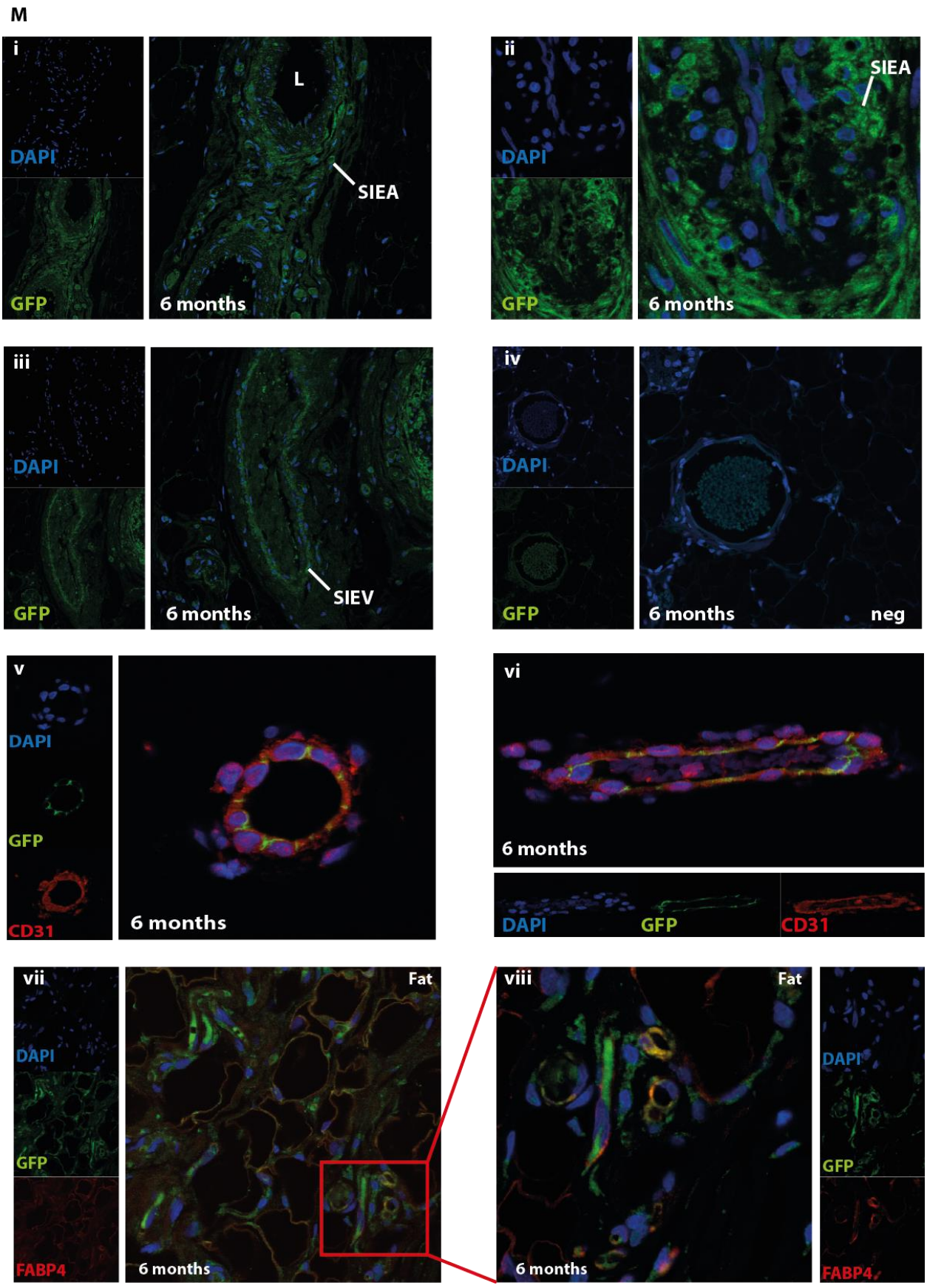
M
i
DAPI
GFP
L
SIEA
6 months
ii
DAPI
GFP
SIEA
6 months
iii
DAPI
GFP
SIEV
6 months
iv
DAPI
GFP
6 months
neg
v
DAPI
GFP
CD31
6 months
vi
6 months
DAPI
GFP
CD31
vii
DAPI
GFP
FABP4
Fat
6 months
viii
Fat
6 months
DAPI
GFP
FABP4

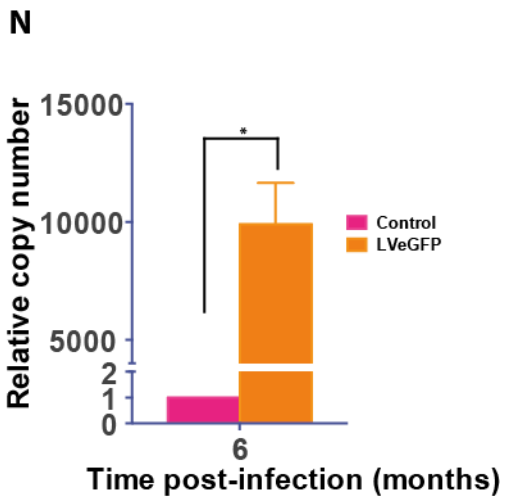

841

842

Fig. 3. *SOD2* over-expression preserves reactive oxygen species scavenging capacity after RT and durable transgene expression can be achieved *in vivo*. A) Graph of SOD2 activity (mean ± SEM) in rat fibroblasts (RF) at 2, 6 and 24 hours after irradiation with 0, 8 or 16 Gy of radiation. The graph shows a dose-dependent reduction in SOD2 activity that occurs earlier with higher radiotherapy doses. **B)** Post-irradiation changes in SOD2 activity in RF cells over-expressing *SOD2* (RF-LVSOD2) compared to vector (RF-LVGFP) and naïve (RF) controls demonstrating significant preservation of SOD2 activity in the RF-LVSOD2 cell line compared to controls. **C)** MTT assays performed using endothelial cells (YPEN1) and endothelial cells over-expressing SOD2 (YPEN1 SOD2) at 120 hours post-irradiation demonstrating significantly greater cell survival in the presence of SOD2 over-expression across a variety of biologically equivalent fractionation schedules. **D)** Three-dimensional spheroid assays using YPEN1 and YPEN1 SOD2 following irradiation across a range of biologically-equivalent fractionation schedules demonstrating significantly greater spheroid volume preservation after RT in cells over-expressing SOD2. **E)** MTT assay (120 hours) investigating the effect of silencing transiently SOD2 expression using siRNA in cells over-expressing SOD2. Control (YPEN1) endothelial cells (ECs) and ECs over-expressing SOD2 were irradiated and demonstrated a survival benefit in cells over-expressing SOD2, which was mitigated by the addition of SOD2 siRNA but not the addition of a scrambled siRNA control. **F)** Confirmation of SOD2 knock-down using siRNA by RT-QPCR demonstrating that SOD2 gene expression was significantly reduced (to almost 10% of basal levels). **G)** i) Quantification of clonogenic assays (mean SF ± SEM) of HeLa and HeLa-LVSOD2 demonstrating a significant increase in SF in HeLa-LVSOD2 at 2 Gy. The trend at 4 and 6 Gy (ii) is suggestive of improved survival in HeLa-LVSOD2. **H)** i) Quantification of clonogenic assays comparing FaDu and FaDu-LVSOD2 (mean SF ± SEM). This graph shows a trend suggestive of greater survival in FaDu-LVSOD2 at all radiation doses (ii). **I)** i and ii) Confocal immunofluorescent microscopy of control and SOD2 over-expressing fibroblasts (RF) using an anti-cytochrome C oxidase antibody (MTCO1) and anti-SOD2 primary antibody demonstrating visible over-expression of SOD2 in the RFSOD2 cells (ii) and co-localization of SOD2 with MTCO1. Cell lysates were collected and split into mitochondrial and cytosolic lysates. Biochemical SOD2 activity was found to be increased significantly in whole cell and mitochondrial lysates of RFSOD2 cells compared to RF controls but this difference did not reach statistical significance for the

cytosolic compartment. **J)** Immunohistochemical staining for SOD2 protein expression in superficial inferior epigastric arteries of flaps infected with LVSOD2 (10^8 TUs) (i) compared with sham (PBS) (ii) controls demonstrating greater protein expression within the vascular compartment. These increases were associated with increased SOD2 activity (iii) and equated to a 50% increase in basal SOD2 activity in flap tissues. SIEA flaps infected with LVSOD2 did not have significantly lower levels of CTGF protein expression (iv) but those infected with both LVSOD2 (10^8 TUs) and LVshCTGF (10^8 TUs) exhibited a significant reduction in CTGF concentration (relative 40% decrease). **K and L)** The flap pedicle, containing only artery and vein, was dissected from the flaps (sham and 10^8 TUs of LVSOD2) and RT-QPCR was performed using pedicle RNA **(K)** to demonstrate significant over-expression of the SOD2 gene in vascular tissues of flaps infected with LVSOD2. This was also associated with significantly increased SOD2 biochemical activity **(L)** in flaps infected with LVSOD2. **M)** Immunofluorescent staining for GFP demonstrating vascular transgene expression at 6 months post-infection with LVeGFP in the SIEA (x 40 (i) and x100 (ii)), SIEV (iii) alongside a negative experimental control (PBS sham infection) (iv). GFP expression was also observed in the microvasculature as demonstrated by co-localization of GFP (green) (v and vi; x100). Nuclei are counter-stained with DAPI (blue). Extra-vascular GFP expression was also observed in the stromal compartment (adipocytes) of the flap as demonstrated by co-localization with fatty acid binding protein 4 (FABP4) (vii (x40) and viii (x100)) at 6 months post-infection (red square represents the area of higher magnification in vii). **N)** Q-PCR for the quantification of viral copy number in SIEA flaps at 6 months post-infection showing that flap infection with 10^8 TUs of LVeGFP results in an approximate 10,000-fold increase in viral copy number compared to un-infected flap tissues. [* $p < 0.05$, ** $p < 0.01$, *** $p < 0.001$, **** $p < 0.0001$].

Fig. S2. Validation of CTGF knock down using LVshCTGF

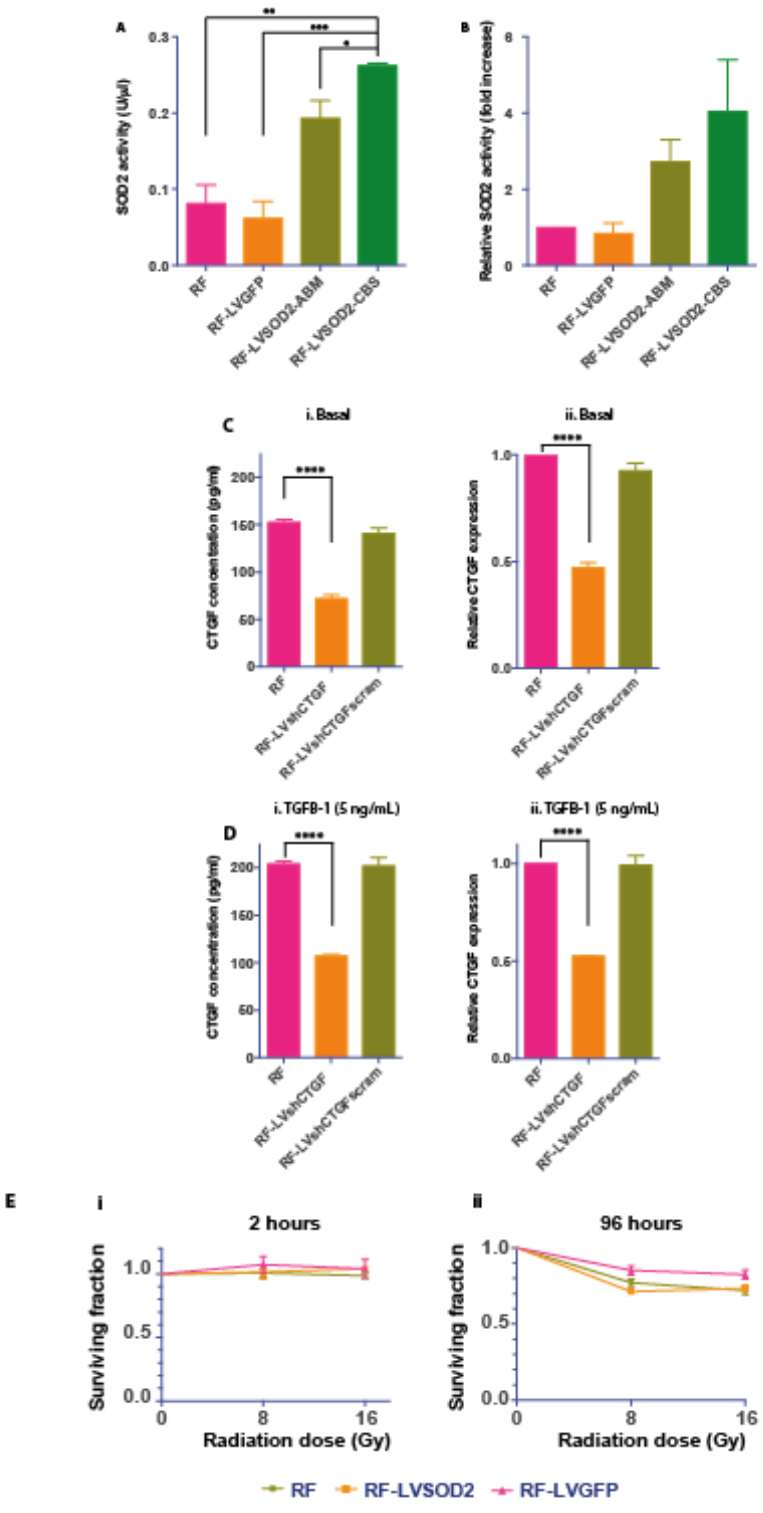

Fig. S2. Validation of CTGF knock down using LVshCTGF. A) SOD2 activity assay (mean ± SEM) comparing two commercially available lentiviral backbones encoding the *SOD2* gene sequence: pLV-III-SOD2-CBS and pLV-III-SOD2-ABM. Lentiviral particles were generated using both plasmids and used to infect RF cells to create 2 different SOD2 over-expressing stable cell lines: RF-LVSOD2-CBS and RF-LVSOD2-ABM. Assaying for SOD2 activity demonstrated significantly greater SOD2 activity in RF-LVSOD2-CBS compared with RF-LVSOD2-ABM. **B)** Relative SOD2 activity, normalized to RF control cells demonstrating that RF-LVSOD2-CBS cells have a 4-fold increase in basal SOD2 activity. **C)** Mean basal CTGF concentrations (± SEM) in absolute (i) and relative (ii) terms across RF controls, RF-LVshCTGF and RF-LVshCTGFscram ($1x10^6$ cells). The data show that LVshCTGF knocks down basal CTGF levels to approximately 50% of control concentrations (ii). **D)** When CTGF expression is stimulated by the exogenous addition of TGFβ-1 (5 ng/mL) infection with LVshCTGF still maintains knock down to 50% of control CTGF concentrations (i and ii). **E)** MTT assay performed at 2 hours after irradiation. Graph displays mean surviving fraction (SF) ± SEM. No differences were observed between control and SOD2 over-expressing cell lines at 2 (i) or 96 (ii) hours post-irradiation with 8 or 16 Gy.

Fig. 4. LVSOD2 and LVshCTGF therapy reduce volume loss and skin contracture following RT

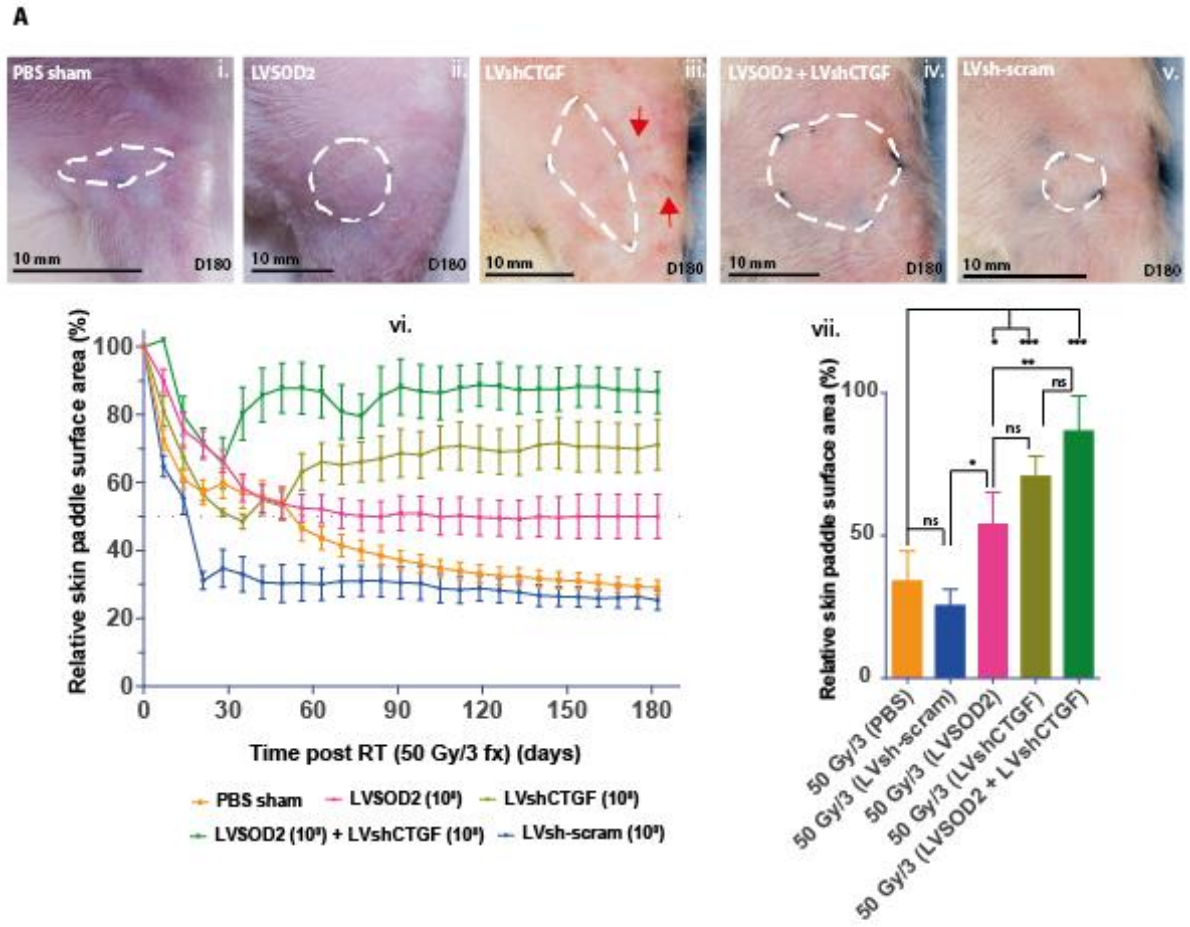

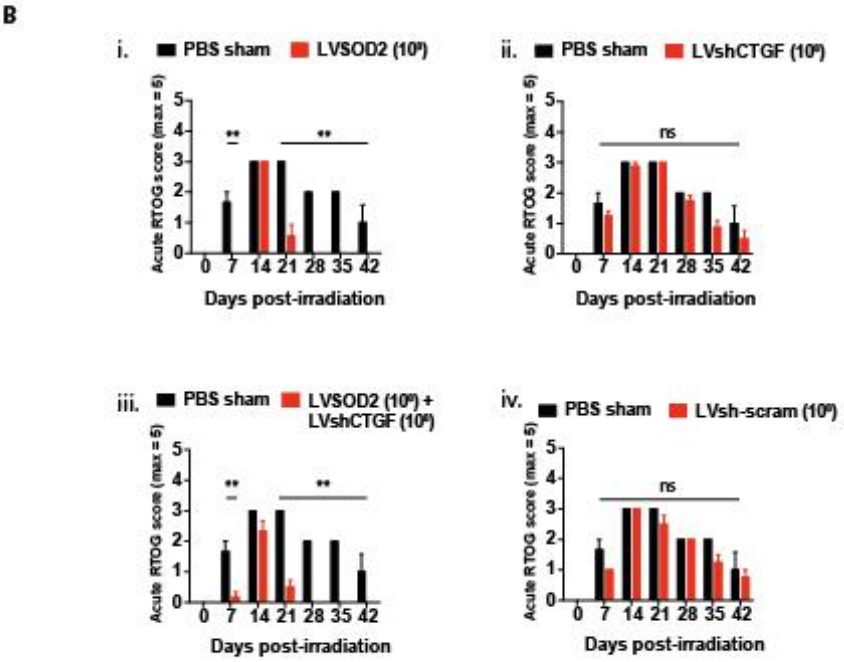

C

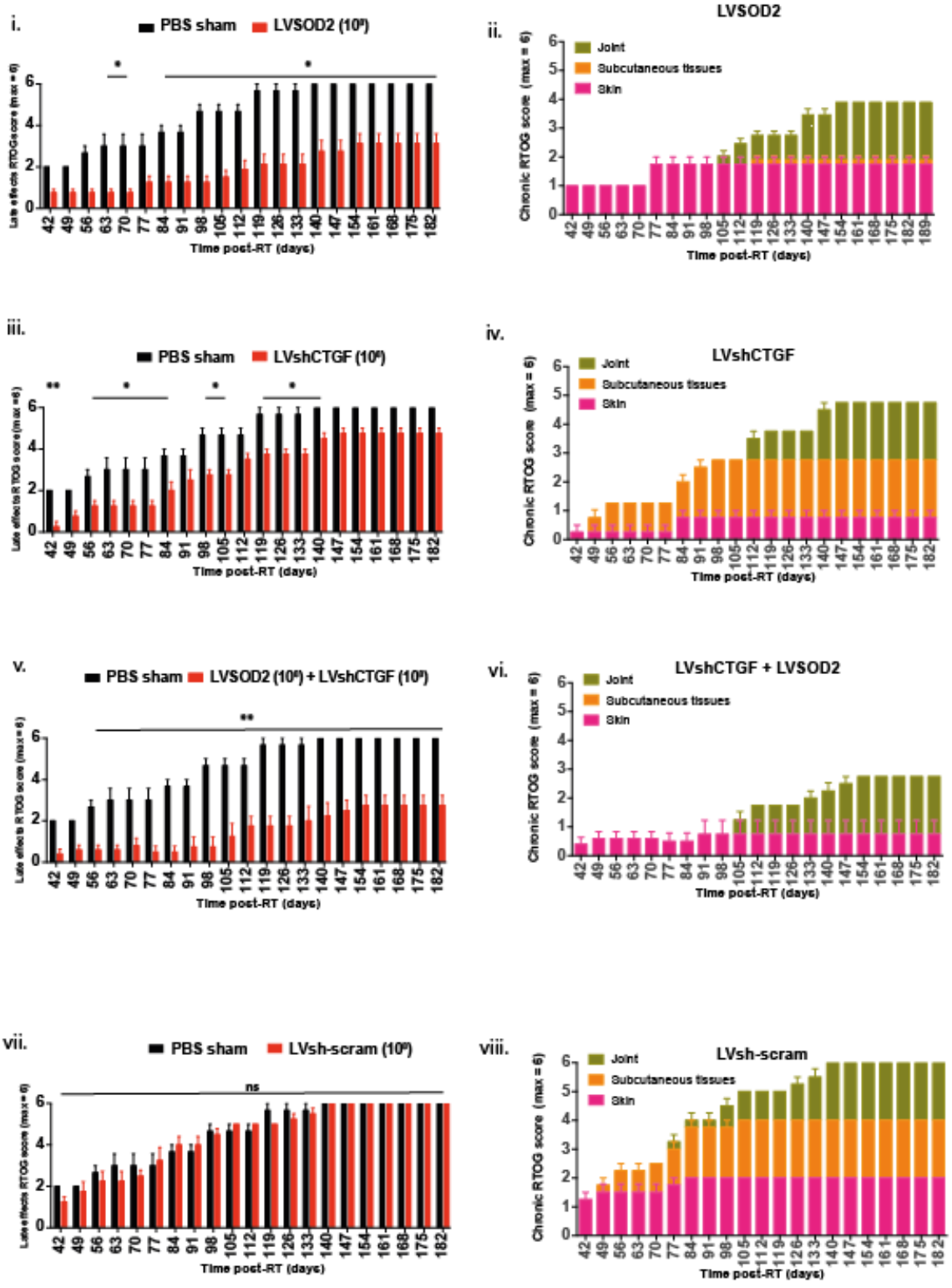
i.
PBS sham
LVSOD2 (10⁸)
Late effects RTOG score (max = 6)
Time post-RT (days)
ii.
LVSOD2
Joint
Subcutaneous tissues
Skin
Chronic RTOG score (max = 6)
Time post-RT (days)
iii.
PBS sham
LVshCTGF (10⁸)
Late effects RTOG score (max = 6)
Time post-RT (days)
iv.
LVshCTGF
Joint
Subcutaneous tissues
Skin
Chronic RTOG score (max = 6)
Time post-RT (days)
v.
PBS sham
LVSOD2 (10⁸) + LVshCTGF (10⁸)
Late effects RTOG score (max = 6)
Time post-RT (days)
vi.
LVshCTGF + LVSOD2
Joint
Subcutaneous tissues
Skin
Chronic RTOG score (max = 6)
Time post-RT (days)
vii.
PBS sham
LVsh-scram (10⁸)
ns
Late effects RTOG score (max = 6)
Time post-RT (days)
viii.
LVsh-scram
Joint
Subcutaneous tissues
Skin
Chronic RTOG score (max = 6)
Time post-RT (days)

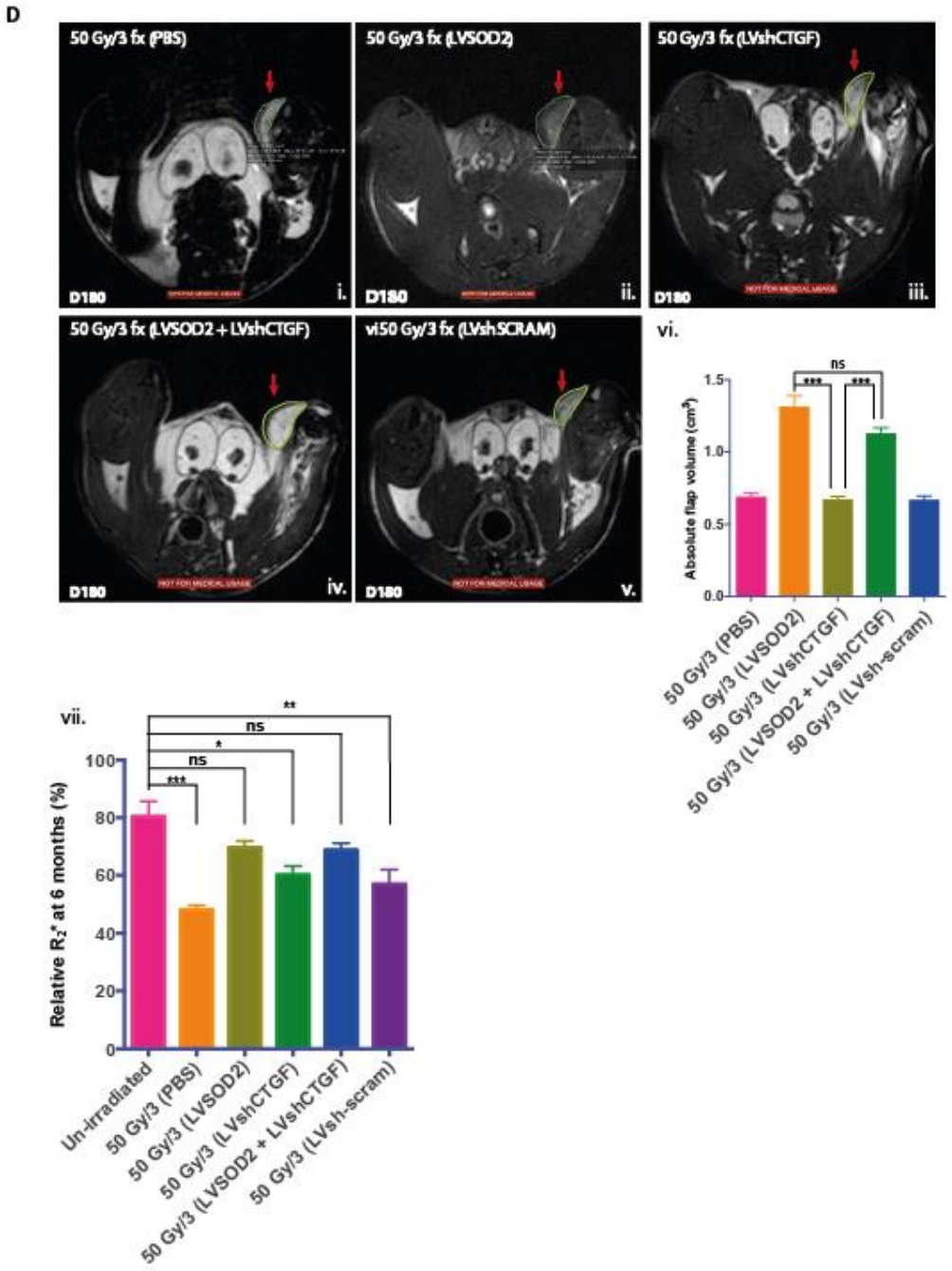

Fig. 4. LVSOD2 and LVshCTGF therapy reduce volume loss and skin contracture following RT. A) Phenotypic appearance of irradiated (50 Gy/3 fractions) SIEA flaps at 180 days following irradiation. Significant improvements in the LAE phenotype were observed in flaps infected with LVSOD2 and LVshCTGF either alone, or, in combination (i-v). Note the appearance of LAEs such as telangiectasia in adjacent tissues into which neither LVSOD2 nor LVshCTGF were delivered (iii red arrows). Quantification of the skin paddle changes (mean skin paddle surface area ± 95% CI) demonstrated significant differences between therapy groups (vi and vii) at 180 days post-irradiation. Specifically, flaps infected with LVSOD2 or LVshCTGF as single agents exhibited significantly less skin paddle contracture than sham (PBS) or vector control (LVscram) infected flaps.

LVshCTGF monotherapy showed a trend towards greater skin paddle preservation compared to LVSOD2 alone however this did not reach statistical significance. Combination therapy with LVSOD2 plus LVshCTGF achieved the greatest improvements in skin paddle contracture with irradiated flaps losing approximately 15% of their pre-irradiation surface area, compared to controls that lost approximately 70%. **B)** RTOG scores for acute toxicities following irradiation demonstrating that flaps infected with LVSOD2 (either alone or in combination) experienced a shorter duration of acute toxicities that resolved sooner (i and iii), however, the maximum severity of acute toxicities was no different between groups. **C)** RTOG severity scoring for LAEs in irradiated flaps (I, iii, v and vii) and RTOG score component breakdown (ii, iv, vi, viii) showing that flaps receiving LVSOD2 monotherapy attained significantly lower RTOG scores for subcutaneous tissue effects (ii). Flaps infected with LVshCTGF achieved lower RTOG scores for cutaneous effects (iv) in the early and intermediate term but these did not persist to the end of the experiment. Flaps receiving dual therapy achieved sustained, lower severity scores for both cutaneous and subcutaneous effects (vi). Of note, no therapeutic group experienced a reduction in severity scores for joint-related effects suggesting that radioprotective effects do not leech out of the flap to its bed. **D)** T_2-weighted *in vivo* MRI of irradiated flaps (red arrows) at 180 days following the cessation of radiotherapy showing that flaps infected with LVSOD2 retained significantly more subcutaneous volume than other therapeutic groups. MRI-derived volumetric analysis (vi) revealed that flaps infected with LVSOD2, either alone or in combination, retained up to 80% of their pre-irradiation volumes, and were also seen to experience significant improvements in relative basal R_2* and were not statistically different from un-irradiated flaps (vii). [*$p<0.05$; **$p<0.01$; ***$p<0.001$].

Fig. 5. Combination therapy with LVSOD2 and LVshCTGF reduces fibrosis post-RT but the preservation of microvascular function is attributable to LVSOD2 only

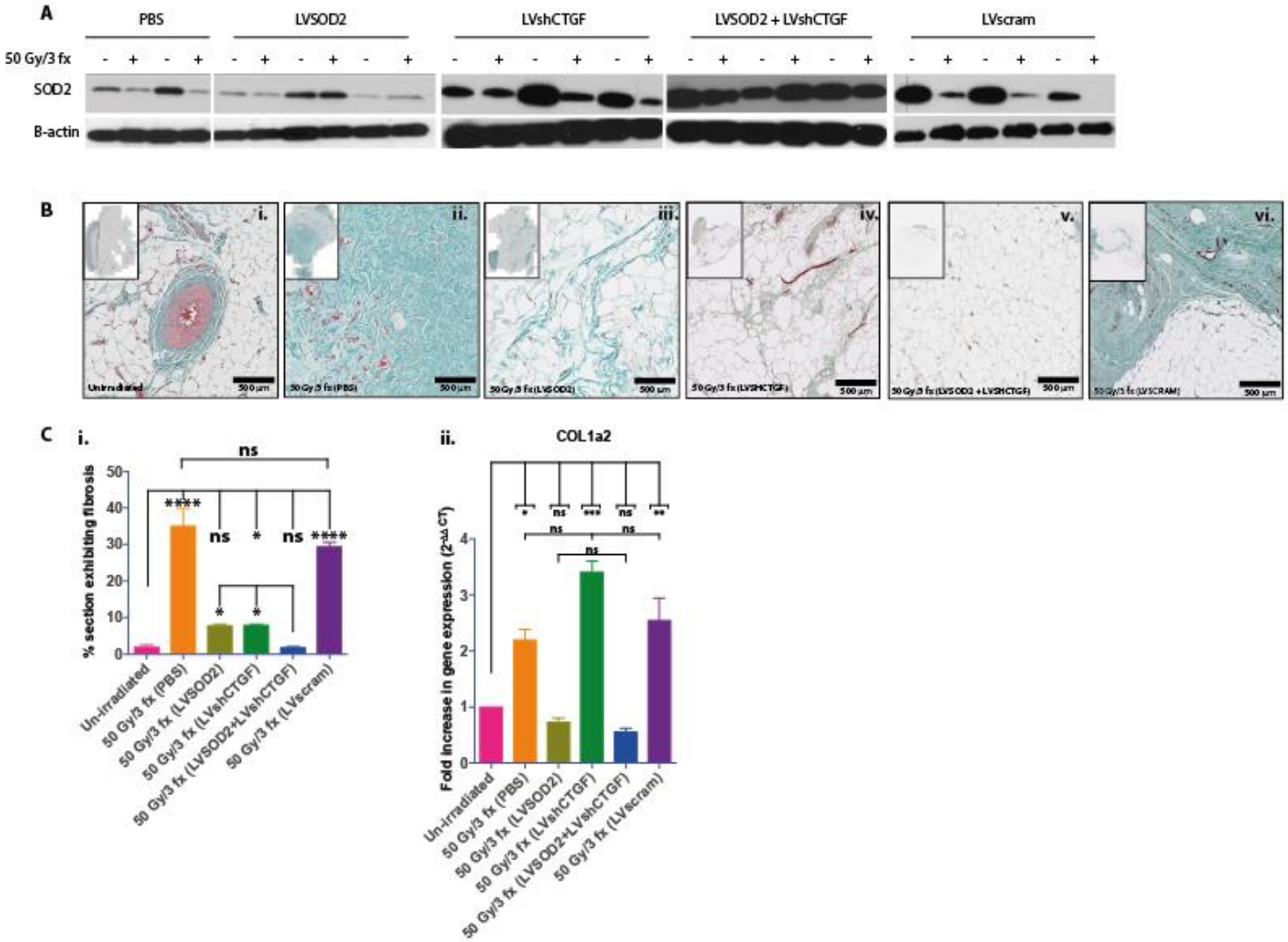

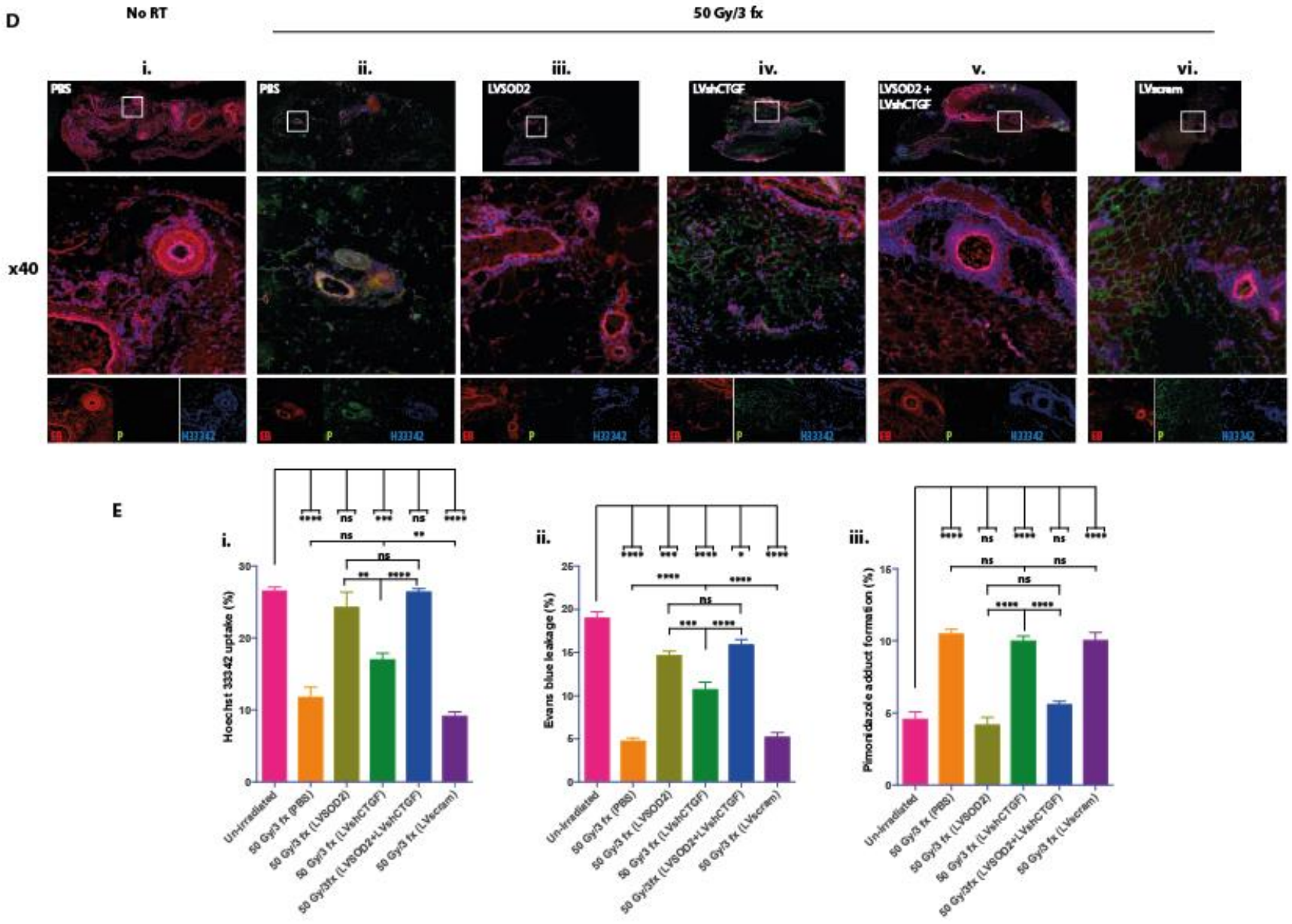
D
No RT
50 Gy/3 fx
i.
ii.
iii.
iv.
v.
vi.
PBS
PBS
LVSOD2
LVshCTGF
LVSOD2 + LVshCTGF
LVscram
x40
EB
P
H33342
E
i.
ii.
iii.
Hoechst 33342 uptake (%)
Evans blue leakage (%)
Pimonidazole adduct formation (%)
Un-irradiated
50 Gy/3 fx (PBS)
50 Gy/3 fx (LVSOD2)
50 Gy/3 fx (LVshCTGF)
50 Gy/3fx (LVSOD2+LVshCTGF)
50 Gy/3 fx (LVscram)
ns

F

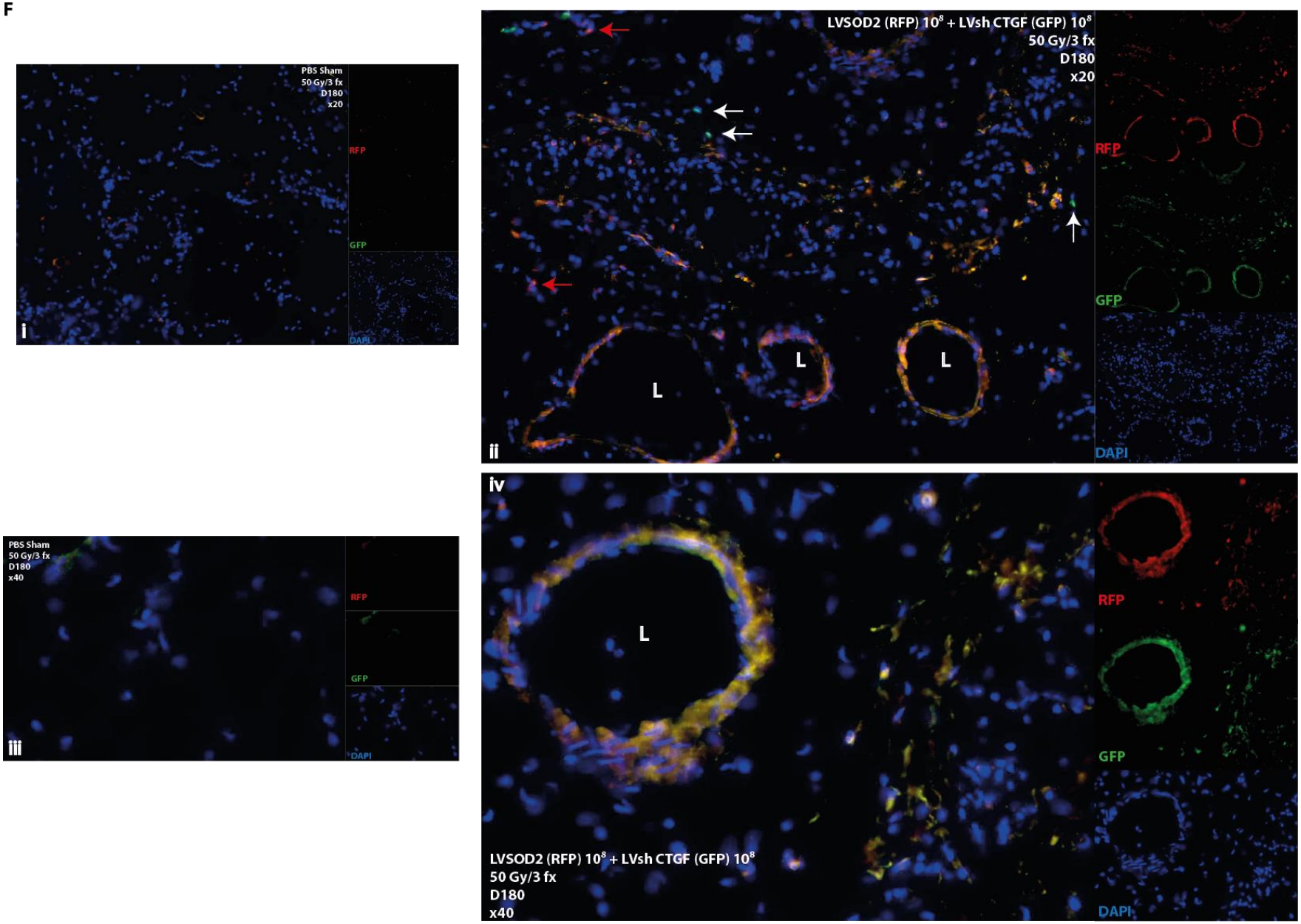
PBS Sham
50 Gy/3 fx
D180
x20
RFP
GFP
DAPI
i
LVSOD2 (RFP) 10^8 + LVsh CTGF (GFP) 10^8
50 Gy/3 fx
D180
x20
L
L
L
ii
PBS Sham
50 Gy/3 fx
D180
x40
iii
LVSOD2 (RFP) 10^8 + LVsh CTGF (GFP) 10^8
50 Gy/3 fx
D180
x40
iv

Fig. 5. Combination therapy with LVSOD2 and LVshCTGF reduces fibrosis post-RT but the preservation of microvascular function is attributable to LVSOD2 only. A) Western blotting for SOD2 in flap tissues taken at 180 days after irradiation with 50 Gy/3 fractions. These data show that the observed reductions in SOD2 expression after RT seen in control groups (PBS and LVscram) are mitigated by the delivery of LVSOD2. Of note, LVshCTGF therapy alone does not appear to impact post-irradiation changes in SOD2 expression. **B)** Masson's trichrome staining for the quantification of fibrosis in flap tissues taken at 180 days after irradiation from each therapeutic group (i-vi). Photos are representative of the larger cohort and whole sections are presented inset (top left). Reductions in collagen deposition (green) were observed in both flaps infected with LVSOD2 and LVshCTGF as monotherapies (iii and iv). Combination therapy with LVSOD2 plus LVshCTGF yielded further reductions in collagen deposition compared to controls (i and vi). **C)** i) Quantification of Masson's trichrome staining showing significant differences in collagen deposition between groups. Specifically, flaps infected with LVSOD2 and LVshCTGF as monotherapies exhibited significantly less fibrosis than controls ($p<0.01$) whereas flaps infected with both vectors exhibited further significant reductions in collagen deposition ($p<0.05$). Correlative RT-QPCR for *Col1a2* gene expression in flap tissues at 180 days post-irradiation demonstrated muting of expression in flaps infected with LVSOD2 (either alone or in combination). LVshCTGF monotherapy resulted in greater *Col1a2* expression compared to sham (PBS) and vector (LVscram) controls ($p<0.05$) but this did not result in greater collagen deposition (figure 6.b.iv). **D)** Immunofluorescent imaging of functional vasculature (Hoechst 33342 (H33342) and Evans blue (EB)) and hypoxia (pimonidazole (P)) in flap tissues taken at 180 days following the end of radiotherapy (i-vi). Images are presented as merged composites (whole section upper panel and x40 middle panel) and split channels (lower panel). These data show differences in H33342, EB and P across therapeutic groups. Specifically, flaps infected with LVSOD2 (either alone or in combination) have preservation of H33342 (viable endothelium) and EB (vascular permeability) and a commensurate reduction in P (hypoxia) staining (iii and v). **E)** Thresholded imaging analysis of immunofluorescent staining for H33342, EB and P demonstrating statistically significant changes. Flaps infected with LVSOD2 (either alone or in combination) showed significant improvements in perfused vasculature (H33342) (i), vascular permeability (EB) (ii) and a reduction in hypoxia (P) (iii). Flaps infected with LVshCTGF showed reductions in perfused vasculature (H33342) (i) and greater hypoxia (P) compared to flaps receiving LVSOD2. However, LVshCTGF flaps showed modest, but significant, improvements in vascular permeability (EB) (ii) compared to sham (PBS) and vector (LVscram) controls. However, these improvements remained significantly less than those seen with LVSOD2 therapy. **F)** Multiplexed immunofluorescent staining for GFP and RFP expression at 180 days post-irradiation in flaps that have been infected with LVSOD2-RFP and LVshCTGF-GFP (10^8 TUs each) and irradiated with 50 Gy/3 fractions. Images are shown alongside negative controls at x20 **(i)** and x40 **(iii)** magnification Images show co-localization of GFP and RFP expression **(ii and iv)**, particularly within vessel walls (L = lumen) but also in the extra-vascular compartment. Cells demonstrating GFP expression alone (white arrows) or RFP expression alone (red arrows) are also observed. [* $p < 0.05$, ** $p < 0.01$, *** $p < 0.001$, **** $p < 0.0001$].

Fig. 6. *SOD2* over-expression in normal tissues does not compromise the cytotoxic efficacy of RT

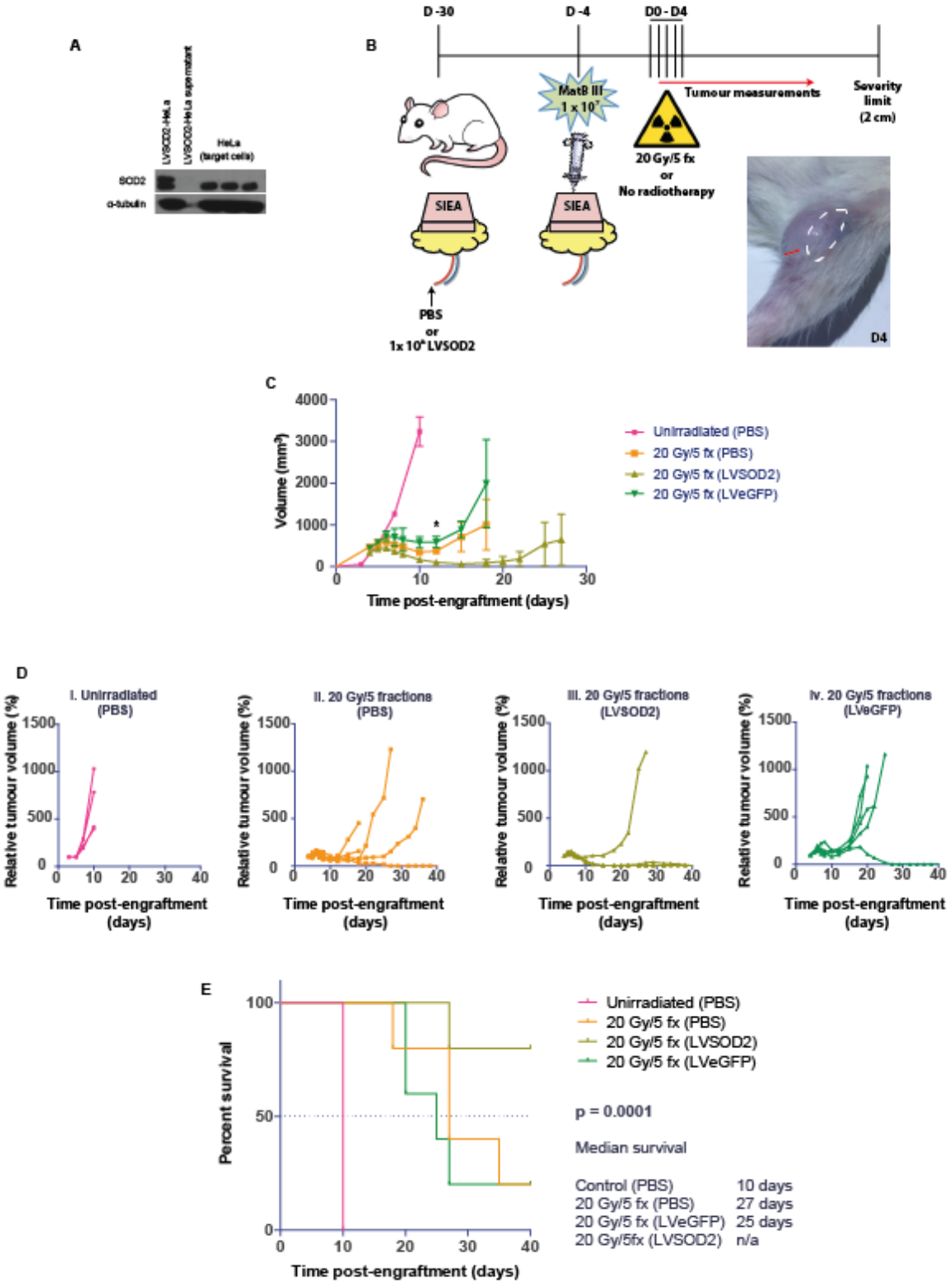

Fig. 6. *SOD2* over-expression in normal tissues does not compromise the cytotoxic efficacy of RT. A) Western blotting for SOD2 to demonstrate that despite SOD2 over-expression (double band) in stable, producer (LVSOD2-HeLa) cells SOD2 over-expression is not seen in naïve target cells following inoculation with media taken from producer cells. **B)** Schematic of the *in vivo* tumour recurrence model using MatBIII cells (rodent breast adenocarcinoma). Animals underwent SIEA flap surgery as described previously, with the delivery of LVSOD2, LVeGFP or sham (PBS). One month later MatBIII cells were engrafted into the flap and established tumours (photo bottom right of panel showing established MatBIII tumour (red arrow) in an SIEA flap (paddle outline dashed white)) were irradiated with 20 Gy/5 fractions (n= 5 animals per group). **C)** Tumour volume growth for MatBIII tumours in flaps infected with LVSOD2, LVeGP or sham (PBS) demonstrating significant differences in tumour volume growth. Following irradiation with 20 Gy/5 fractions tumours growing in LVSOD2-infected flaps exhibited significantly slower tumour growth compared to those growing in flaps infected with control vectors. **D)** Individual growth curves for tumours growing in: sham (PBS) infected and un-irradiated (i), sham (PBS) infected and irradiated (20Gy/5 fractions) (ii), LVSOD-infected and irradiated (20 Gy/5 fractions) (iii) and LVeGFP-infected and irradiated (20 Gy/5 fractions) (iv). These data show that 4 out of 5 tumours irradiated in LVSOD2-infected flaps achieved remission whereas only 1 out of 5 tumours in each control group (sham (PBS) and vector (LVeGFP)) achieved remission. **E)** Kaplan-Meier plot of survival to humane end-point for animals with MatBIII tumours grown in sham (PBS), LVSOD2 or LVeGFP flaps showing significant differences in survival. Animals with LVSOD2-infected flaps did not achieve median survival whereas animals with control (sham (PBS) or vector (LVeGFP)) flaps had significantly shorter median survival (PBS: 27 days, LVeGFP: 25 days).

Supplementary Materials:

Supplementary methods

Immunohistochemistry

In vivo specimens were fixed in formalin for 24 hours after harvest, embedded and mounted. Sections for immunohistochemical analysis were cut at 3 μm thickness. Sections were de-waxed, washed and antigen retrieval performed (CTGF: 97°C for 20 min in pH 6 citrate buffer (Dako S2031, Ely, UK); SOD2: pressure cook for 2 min in pH 6 citrate buffer (Dako S2031); PTEN: 97°C for 20 min in pH 6 citrate buffer (Dako S2031)). Sections were rinsed in wash buffer (Dako S3006) and endogenous peroxidases blocked (Dako S2023). Sections were incubated with primary antibody (CTGF (1:500; Abcam, Cambridge, UK), SOD2 (1:400; Abcam, Cambridge, UK) and PTEN (1:100; Cell Signalling Technologies, Leiden, Denmark)) in antibody diluent (Dako S2022) for 1 hour at room temperature. Sections were washed and Dako Envision HRP Polymer (K4011) applied for 30 minutes at room temperature. Immunostaining was then visualized using liquid DAB (3,3'-diaminobenzidine) (Dako) substrate for 5 minutes before sections were washed, counterstained with haematoxylin (CellPath, Newton, Wales) and mounted. For Masson's trichrome staining, Weigerts haematoxylin A and B (TCS Bioscience, Buckingham, UK) were mixed in a 1:1 ratio and applied to sections for 5 minutes. Sections were washed and stained using the Masson's Trichrome light green kit (TCS Bioscience). For CTGF, SOD2 and PTEN immunohistochemical staining, counts were performed in three x 20 fields in 3 non-consecutive sections of tissue per *in vivo* sample. For CTGF, SOD2 and PTEN, positivity was defined by the presence of membranous or cytoplasmic staining. Fibrosis was quantified by as the percentage of the whole section exhibiting fibrotic change using post-hoc imaging software (Image J, NIH, Bethesda, USA).

Immunofluorescence

Sections were de-waxed, rehydrated, permeabilized in 0.2% Triton detergent (Sigma-Aldrich, Gillingham, UK) and blocked with IFF for 1 hour. Sections were then incubated with primary antibody (anti-eGFP (rabbit polycloncal 1:100, Abcam, Cambridge UK) at 4°C overnight. Co-staining was performed using anti-CD31 (mouse polyclonal 1:100, Novus Biologicals, Cambridge, UK) and anti-FABP4 (fatty acid binding protein 4) (mouse polyclonal 1:200, R and D Systems, Abingdon, UK) with anti-eGFP. The following day, sections were washed in PBS and incubated with a goat anti-rabbit 488 (eGFP) and/or chicken anti-mouse 555 (CD31 and FABP4) FITC-conjugated secondary antibody (1:1000 in IFF) (Life Technologies, Paisley, UK) for 1 hour at room temperature and then washed in PBS with 4',6-diamidino-2-phenylindole (DAPI; 1:50,000; Sigma-Aldrich, Gillingham, UK). Sections were then rinsed and fixed in paraformaldehyde (4%) for 15 minutes. Confocal images were captured on a Leica Microsystems TCS-SP2 confocal (Leica Microsystems, Milton Keynes, UK). Controls sections included experimental controls (SIEA flaps that had not been infected with LVeGFP) and staining controls (LVeGFP-infected flaps incubated with either primary or secondary antibody only). Three non-consecutive sections from each sample were examined by fluorescence microscopy.

Multi-plexed immunofluorescent imaging

Frozen sections were fixed on the slide with 4% PFA, subjected to antigen retrieval in Citrate buffer (10mM Sodium Citrate Buffer, 0.05% Tween 20, pH 6.0) and blocked with rabbit/mouse serum for 10 mins before application of anti GFP antibody (Abcam, Cambridge, UK) at a concentration of 1in100, at room temperature for 30 minutes. Slides were washed 3x in TBST before addition of anti-rabbit/mouse HRP conjugated secondary antibody (Perkin Elmer) for 10 minutes. Slides were washed again 3x, before addition of Opal HRP substrate (Perkin Elmer) for 20 minutes. Upon completion of the first staining, antibodies were stripped by 2 minutes antigen retrieval in Citrate buffer and the whole staining process repeated for RFP antibody (Abcam, Cambridge, UK) (1 in 100). Stained sections were imaged using a Vectra 3.0 multispectral microscope (Perkin Elmer).

Cell lines

Immortalized rat fibroblasts (RFs) (kind gift from Prof Tony Ng, King's College, London), HeLa (human uterine cervical adenocarcinoma) and FaDu (human hypopharyngeal squamous cell carcinoma) cells were maintained in DMEM supplemented with 10% foetal calf serum (BD Biosciences, Oxford, UK), 2 mM l-arginine (CSSD, ICR) and 1% penicillin/streptomycin (CSSD, ICR). Rat MatB IIIbreast adenocarcinoma cells (ATCC, Teddington, UK) were maintained in McCoy's 5A (modified) medium (Gibco®, Life Technologies Inc., Paisley, UK) supplemented with 10% FCS, 2 mM l-arginine and 1% penicillin/streptomycin. Cells were cultured in a humidified incubator at 37°C (95% air, 5% CO_2). Cells were routinely tested for the presence of mycoplasma infection.

Generation of stable cell lines

Target cells were plated at between 1-5 x 10^5 cells per 6 cm or 10 cm tissue culture dish 24 hours prior to infection with lentivirus. The following day, medium was aspirated from the target cells and a lentiviral inoculum (1-5 mL) was added to the cells with fresh DMEM (+10% DMEM) and polybrene (1 μg/mL). The following day the inoculum was aspirated and replaced with fresh medium. After 72 hours, puromycin at a concentration ranging from 0.5-20 μg/mL was added to the medium to select for infected cells. Cells were propagated, thereafter, in medium with puromycin.

Protein quantification

Protein concentration of the lysates was determined using the Bicinchoninic Acid (BCA) Protein Assay Reagent (Pierce, Rockford, IL). Reagents and samples were combined as per the manufacturers instructions and absorbances read at 570 nm (SpectraMax, Sunnyvale, CA, USA). Protein concentrations were derived from an albumin standard as per the manufacturer's protocol.

Western blotting

Thirty micrograms of lysate was mixed with 7.5 μL Laemmeli buffer (Sigma-Aldrich, Gillingham, UK) and made up to a total volume of 25 μL with sterile water. Samples were then heated at 95°C for 5 minutes and loaded onto SDS polyacrylamide gels (10% Bis-Tris) (Life Technologies Inc., Paisley, UK) running in MOPS buffer (Life Technologies Inc., Paisley, UK).

Electrophoresis was performed at 100 volts (V) at room temperature. Proteins were transferred onto a polyvinylidenedifluoride (PVDF) Hybond-P membrane (0.45 μm) (Amersham, Arlington Heights, IL) using a wet transfer protocol in transfer buffer (192 mM glycine, 25 mM Tris and 200 mM methanol (CSSD, ICR) at pH 8.3). Following this, membranes were rinsed in Tris-buffered saline containing 0.1% TWEEN-20 (Sigma-Aldrich, Gillingham, UK) (TBS-TWEEN) and then blocked in a 5% milk solution (5 g powdered milk in 100 mL TBS-TWEEN).

Immunodetections were performed using a variety of primary antibodies incubated overnight with membranes in a 5% milk solution. The following day, membranes were washed, incubated with the appropriate secondary antibody (sheep anti-mouse IgG or donkey anti-rabbit rabbit IgG (1:1000 (ECL™, GE Healthcare Ltd., Bedford, UK) (in 5% milk solution) for 1 hour at room temperature and washed once more. Detections were carried out using the Immobilon Western chemoluminescent horseradish peroxidase (HRP) substrate (Millipore, Watford, UK). Membranes were exposed to photographic films (Fujifilm Global, Tokyo, Japan) and developed. Equal loading was assessed using β-actin or α-tubulin (Sigma) mouse monoclonal primary antibodies.

SOD2 activity assay

Assays were performed using a high throughput SOD2 assay (Sigma Aldrich, Gillingham, UK) as per the manufacturer's protocol. The assay relies upon the competitive inhibition of reactive oxygen species (ROS), generated in the reaction mix, by endogenous SOD2 to effect a colorimetric change. Formation. The assay was performed using 20 μL of *in vitro* or *in vivo* samples (0.5 μg/μL) per well of a 96-well plate. Samples were mixed with 200 μL of a Wst-working solution and 20 μL of xanthine oxidase (XO) was added. Standard wells were also set up with the omission of either the sample solution, enzyme working solution or both of these. Plates were incubated at 37°C for 20 minutes and absorbance was then read at 450 nm using a spectrophotometer. SOD2 activity was calculated as the "% inhibition", which represents SOD2 activity relative to the standard wells.

SOD2 siRNA transient knock down

SiRNA knockdown against human SOD2 was performed using Dharmacon ON-TARGETplus SOD2 siRNA and appropriate ON-TARGETplus SMARTPool controls (Dharmacon, GE Healthcare, UK) in accordance with the manufacturer's protocols. In brief, 1 x 10^5 YPEN1-SOD2 overexpressing cells were plated onto six well culture plates (NUNC, ThermoFisher Scientific, UK), in complete DMEM supplemented with 10% FCS (The Institute of Cancer Research, London, UK). The next day, 10μl of 5μM SiRNA was diluted with 190μl serum-free Optimem (Glibco, ThermoFisher Scientific, UK), and incubated with 2μl of Lipofectamine RNAiMAX transfection reagent (Thermo Fisher Scientific, UK) diluted in 198μl Optimem for 20 minutes at room temperature. This was added to 1600μl of complete DMEM 10% FCS, mixed adequately and used to replace the media on the plates. 24 hours later the media was replaced with 2ml of complete DMEM 10% FCS and the cells used for experiments.

CTGF ELISA

A commercially-available ELISA for CTGF was used (Peprotech Ltd., London, UK) and assays were performed as per the manufacturer's instructions. In brief, 100 μL of a capture antibody solution (1 μg/mL) was plated per well of a 96-well plate (R and D Systems, Abingdon, UK) and left to incubate overnight at room temperature. The following day, the capture antibody was discarded and the plate washed and blocked with a sterile-filtered, blocking solution (PBS + 1% bovine serum albumin (Sigma-Aldrich, Gillingham, UK)) for 1 hour at room temperature and washed again. Samples were loaded in triplicate on the plate alongside a CTGF standard (range: 62.5 – 4,000 pg/mL) and left to incubate at room temperature for 2 hours. The plate was then washed and a solution of biotinylated-detection antibody (0.5 μg/mL, 100 μL/well) added to each well and left to incubate for 2 hours. The plate was washed once more and 100 μL of an avidin solution (6 μL of a stock solution diluted in 12 mL of diluent (PBS + 0.1% BSA + 0.05% TWEEN)) added to each well and left to incubate for half an hour. One hundred microlitres of ABTS (2,2′-Azino-bis(3-ethylbenzothiazoline-6-sulfonic acid) liquid substrate (Sigma-Aldrich, Gillingham, UK) was added to each well and absorbance was read (at 450 nm with a wavelength correction set to 650 nm) at 5 minute-intervals for 45 minutes. Data analysis was performed as per the manufacturer's instructions using readings obtained from the CTGF standards to extrapolate CTGF concentrations within samples.

3-(4,5-dimethylthiazol-2-y)-2,5-diphenyltetrazolium bromide (MTT) assay

5 x 10^4 cells were plated per well of a 96-well plate and allowed to attach prior to irradiation. At the experimental end points (24 and 96 hours), 20 μL of MTT (Sigma-Aldrich, Gillingham, UK) was added to each well and the plate incubated for 4 hours. At this point, the medium was aspirated and 200 μL of 100% DMSO solution was added to each well. Plates were placed on a rocker to facilitate dissolution of MTT crystals and 1 hour later absorbances were read at 550 nm using a spectrophotometer.

Clonogenic assay

To investigate longer-term survival following irradiation, cells were plated at a range of seeding densities in separate wells of a 6-well plate. The following day, cells were irradiated with 0, 2, 4 or 6 Gy and incubated at 37°C for 10 to 14 days thereafter. At this time, the medium was discarded and colonies fixed with a crystal violet solution (0.2% crystal violet, 0.7% ethanol). Clonogenic assays were quantified digitally using CellProfiler 2.0 (Broad Institute, Cambridge MA, USA). Briefly images were converted to greyscale, contrast enhanced to make colonies more distinct from background and inverted for processing with CellProfiler. Quantification measured the average plating efficiency from duplicate wells per experiment, with a minimum of three independent experiments per condition. Surviving fractions were calculated from the control plating efficiencies for independent repeats.

Spheroid assay

5x10^4 cells per well were plated in U-bottom low attachment plates (Corning, NY, USA). 96 h after plating spheroids were irradiated. Radiation doses used were either 5 Gy or 8 Gy radiation in a single fraction on day 1, or three 2.4 and 4.15 Gy fractions on consecutive days 1-3. Media was changed three times per week. Spheroids were imaged and automated area quantification performed at day 12 using a Celigo S high throughput micro-well image cytometer (Nexcelom, MA, USA). Values were adjusted relative to the average area of the control spheroid

group. A minimum of 11 spheroid measurements per condition were quantified across two biologically independent repeats.

Polymerase chain reaction (PCR)

RNA and genomic DNA (gDNA) were extracted from 0.1 g of flap tissue using commercially-available nucleic acid extraction kits (Qiagen RNeasy kit and DNeasy Blood and Tissue kit, Qiagen, Hilden, Germany). All extractions were performed as per the manufacturer's instructions. cDNA synthesis was performed using the RT^2 First Strand cDNA synthesis kit (Sabiosciences, Crawley, UK). In brief, 500 ng of extracted RNA was mixed with 2 μL buffer GE and made up to a volume of 10 μL using RNase-free water. This was incubated at 42°C for 15 minutes to eliminate gDNA and then placed on ice for 1 minute. A reverse transcription mix was made using: 4 μL 5 x Buffer BC2, 1 μL control P2, 2 μL RE3 reverse transcriptase mix and 3 μL RNase-free water (total volume = 10 μL). The genomic elimination mix (10 μL) was mixed with the reverse-transcription mix and pipetted up and down. This was then incubated at 42°C for 15 minutes to allow for reverse transcription. The reaction was stopped by incubating the mix at 95°C for 5 minutes and 91 μL of RNase-free water added.

PCR for CTGF, Col1a2, Col3a1 and SOD2

RT-QPCR using primers for *CTGF*, *Col1a2*, *Col3a1*, *SOD2* and *β-actin* (QuantiTect Primer Assays, Qiagen, Hilden, Germany) was performed. Reactions were performed using 50 ng of cDNA mixed with 2 μL primer solution (20 μM) and made up to a volume of 10 μL with RNase-free water. Reactions were amplified using SYBR Green and the StepOne™ Q-PCR system (Applied Biosciences, Life Technologies, Paisley, UK). Amplification was performed under the following cycling conditions: 95°C 10 minutes (1 cycle) (denaturing), 95°C 10 s→58°C 10 s→72°C 10 s (40 cycles) (quantification), 40°C 20 s (1 cycle) (cooling). Changes in expression were calculated using the ddCT method and reported normalized to housekeeping genes (β-actin).

PCR for viral DNA

Quantitative PCR (Q-PCR) using primers targeted against the 5' end of the *gag* gene was performed to quantify the presence of viral DNA in infected flap tissues. The primer sequences were obtained from Capital Biosciences (Rockville, USA). 100 ng of gDNA was mixed with 0.5 μL of forward (FW) and reverse (RV) primers (*gag*: FW: 5'-GGAGCTAGAACGATTCGCAGTTA-3'; RV: 5'-GGTTGTAGCTGTCCCAGTATTTG-3';), 2 μL SYBR Green mastermix and made up to a volume of 20 μL DNase/RNase-free water. Commercially-available primers for rat β-actin (QuantiTect Primer Assays, Qiagen, Hilden, Germany) were also used to standardize quantification to a housekeeping gene. PCR amplification was performed under the following cycling conditions: 95°C for 10 minutes (1 cycle) (denaturing), 95°C 10 s→60°C 10 s→72°C 25 s (45 cycles) (quantification), 95°C→65°C 1 minute→95°C (1 cycle) (melting), 40°C 30 s (1 cycle) (cooling). Gene copy number was calculated using the ddCT method using β-actin as a housekeeping gene.

References and Notes:

1. T. J. Whelan, J. P. Pignol, M. N. Levine, J. A. Julian, R. MacKenzie, S. Parpia, W. Shelley, L. Grimard, J. Bowen, H. Lukka, F. Perera, A. Fyles, K. Schneider, S. Gulavita, C. Freeman, Long-term results of hypofractionated radiation therapy for breast cancer. *N Engl J Med* **362**, 513-520 (2010); published online EpubFeb 11 (10.1056/NEJMoa0906260).
2. G. Danish Breast Cancer Cooperative, H. M. Nielsen, M. Overgaard, C. Grau, A. R. Jensen, J. Overgaard, Study of failure pattern among high-risk breast cancer patients with or without postmastectomy radiotherapy in addition to adjuvant systemic therapy: long-term results from the Danish Breast Cancer Cooperative Group DBCG 82 b and c randomized studies. *Journal of clinical oncology : official journal of the American Society of Clinical Oncology* **24**, 2268-2275 (2006); published online EpubMay 20 (10.1200/JCO.2005.02.8738).
3. A. H. Chao, D. W. Chang, S. W. Shuaib, M. M. Hanasono, The Effect of Neoadjuvant versus Adjuvant Irradiation on Microvascular Free Flap Reconstruction in Sarcoma Patients. *Plastic and reconstructive surgery* **129**, 675--682 (2012).
4. M. N. Mirzabeigi, J. M. Smartt, J. A. Nelson, J. Fosnot, J. M. Serletti, L. C. Wu, An Assessment of the Risks and Benefits of Immediate Autologous Breast Reconstruction in Patients Undergoing Postmastectomy Radiation Therapy. *Annals of Plastic Surgery* **71**, 149--155 (2013).
5. N. E. Rogers, R. J. Allen, Radiation effects on breast reconstruction with the deep inferior epigastric perforator flap. *Plastic and reconstructive surgery* **109**, 1919--1924-- discussion 1925--1916 (2002).
6. S. J. Kronowitz, Current Status of Autologous Tissue--Based Breast Reconstruction in Patients Receiving Postmastectomy Radiation Therapy. *Plastic and reconstructive surgery* **130**, 282--292 (2012).
7. D. H. Rochlin, A. R. Jeong, L. Goldberg, T. Harris, K. Mohan, S. Seal, J. Canner, J. M. Sacks, Postmastectomy radiation therapy and immediate autologous breast reconstruction: integrating perspectives from surgical oncology, radiation oncology, and plastic and reconstructive surgery. *J Surg Oncol* **111**, 251-257 (2015); published online EpubMar (10.1002/jso.23804).
8. R. Gurunluoglu, A. Gurunluoglu, S. A. Williams, S. Tebockhorst, Current trends in breast reconstruction: survey of American Society of Plastic Surgeons 2010. *Ann Plast Surg* **70**, 103-110 (2013); published online EpubJan (10.1097/SAP.0b013e31822ed5ce).
9. A. Elkowitz, S. Colen, S. Slavin, J. Seibert, M. Weinstein, W. Shaw, Various methods of breast reconstruction after mastectomy: an economic comparison. *Plast Reconstr Surg* **92**, 77-83 (1993); published online EpubJul (
10. A. Khoo, S. S. Kroll, G. P. Reece, M. J. Miller, G. R. Evans, G. L. Robb, B. J. Baldwin, B. G. Wang, M. A. Schusterman, A comparison of resource costs of immediate and delayed breast reconstruction. *Plast Reconstr Surg* **101**, 964-968; discussion 969-970 (1998); published online EpubApr (
11. S. S. Kroll, J. A. Coffey, Jr., R. J. Winn, M. A. Schusterman, A comparison of factors affecting aesthetic outcomes of TRAM flap breast reconstructions. *Plast Reconstr Surg* **96**, 860-864 (1995); published online EpubSep (
12. S. K. Al-Ghazal, L. Sully, L. Fallowfield, R. W. Blamey, The psychological impact of immediate rather than delayed breast reconstruction. *European journal of surgical oncology : the journal of the European Society of Surgical Oncology and the British Association of Surgical Oncology* **26**, 17-19 (2000); published online EpubFeb (
13. J. Tall, T. C. Bjorklund, A. C. Skogh, C. Arnander, M. Halle, Vascular Complications After Radiotherapy in Head and Neck Free Flap Reconstruction: Clinical Outcome Related to Vascular Biology. *Ann Plast Surg* **75**, 309-315 (2015); published online EpubSep (10.1097/SAP.0000000000000081).
14. M. Halle, M. Ekstrom, F. Farnebo, P. Tornvall, Endothelial activation with prothrombotic response in irradiated microvascular recipient veins. *Journal of plastic, reconstructive & aesthetic surgery : JPRAS* **63**, 1910-1916 (2010); published online EpubNov (10.1016/j.bjps.2009.12.001).
15. E. Rannou, A. Francois, A. Toullec, O. Guipaud, V. Buard, G. Tarlet, E. Mintet, C. Jaillet, M. L. Iruela-Arispe, M. Benderitter, J. C. Sabourin, F. Milliat, In vivo evidence for an endothelium-dependent mechanism in radiation-induced normal tissue injury. *Scientific reports* **5**, 15738 (2015); published online EpubOct 29 (10.1038/srep15738).
16. H. E. Barker, J. T. Paget, A. A. Khan, K. J. Harrington, The tumour microenvironment after radiotherapy: mechanisms of resistance and recurrence. *Nature reviews. Cancer* **15**, 409-425 (2015); published online EpubJul (10.1038/nrc3958).
17. C. B. Westbury, J. R. Yarnold, Radiation Fibrosis - Current Clinical and Therapeutic Perspectives. *Clinical Oncology*, 1--16 (2012).

18. J. Yarnold, M.-C. V. Brotons, Pathogenetic mechanisms in radiation fibrosis. *Radiotherapy and Oncology* **97**, 149--161 (2010).
19. M. W. Epperly, C. A. Sikora, S. J. DeFilippi, J. E. Gretton, D. Bar-Sagi, H. Archer, T. Carlos, H. Guo, J. S. Greenberger, Pulmonary irradiation-induced expression of VCAM-I and ICAM-I is decreased by manganese superoxide dismutase-plasmid/liposome (MnSOD-PL) gene therapy. *Biology of blood and marrow transplantation : journal of the American Society for Blood and Marrow Transplantation* **8**, 175-187 (2002).
20. E. Mintet, E. Rannou, V. Buard, G. West, O. Guipaud, G. Tarlet, J. C. Sabourin, M. Benderitter, C. Fiocchi, F. Milliat, A. Francois, Identification of Endothelial-to-Mesenchymal Transition as a Potential Participant in Radiation Proctitis. *Am J Pathol* **185**, 2550-2562 (2015); published online EpubSep (10.1016/j.ajpath.2015.04.028).
21. S. H. Choi, Z. Y. Hong, J. K. Nam, H. J. Lee, J. Jang, R. J. Yoo, Y. J. Lee, C. Y. Lee, K. H. Kim, S. Park, Y. H. Ji, Y. S. Lee, J. Cho, Y. J. Lee, A Hypoxia-Induced Vascular Endothelial-to-Mesenchymal Transition in Development of Radiation-Induced Pulmonary Fibrosis. *Clinical cancer research : an official journal of the American Association for Cancer Research* **21**, 3716-3726 (2015); published online EpubAug 15 (10.1158/1078-0432.CCR-14-3193).
22. S. Piera-Velazquez, F. A. Mendoza, S. A. Jimenez, Endothelial to Mesenchymal Transition (EndoMT) in the Pathogenesis of Human Fibrotic Diseases. *Journal of clinical medicine* **5**, (2016); published online EpubApr 11 (10.3390/jcm5040045).
23. M. Carpenter, M. W. Epperly, A. Agarwal, S. Nie, L. Hricisak, Y. Niu, J. S. Greenberger, Inhalation delivery of manganese superoxide dismutase-plasmid/liposomes protects the murine lung from irradiation damage. *Gene Ther* **12**, 685-693 (2005); published online EpubApr (10.1038/sj.gt.3302468).
24. M. W. Epperly, J. E. Gretton, C. A. Sikora, M. Jefferson, M. Bernarding, S. Nie, J. S. Greenberger, Mitochondrial Localization of Superoxide Dismutase is Required for Decreasing Radiation-Induced Cellular Damage. *Radiation Research* **160**, 568--578 (2003).
25. J. S. Greenberger, M. W. Epperly, Review. Antioxidant gene therapeutic approaches to normal tissue radioprotection and tumor radiosensitization. *In Vivo* **21**, 141-146 (2007); published online EpubMar-Apr (
26. X. Zhang, M. W. Epperly, M. A. Kay, Z. Y. Chen, T. Dixon, D. Franicola, B. A. Greenberger, P. Komanduri, J. S. Greenberger, Radioprotection in vitro and in vivo by minicircle plasmid carrying the human manganese superoxide dismutase transgene. *Hum Gene Ther* **19**, 820-826 (2008); published online EpubAug (10.1089/hum.2007.141).
27. D. L. Tribble, M. H. Barcellos-Hoff, B. M. Chu, E. L. Gong, Ionizing radiation accelerates aortic lesion formation in fat-fed mice via SOD-inhibitable processes. *Arteriosclerosis, thrombosis, and vascular biology* **19**, 1387-1392 (1999); published online EpubJun (
28. M. Epperly, J. Bray, S. Kraeger, R. Zwacka, J. Engelhardt, E. Travis, J. Greenberger, Prevention of late effects of irradiation lung damage by manganese superoxide dismutase gene therapy. *Gene Therapy* **5**, 196--208 (1998).
29. M. W. Epperly, J. A. Bray, P. Esocobar, W. L. Bigbee, S. Watkins, J. S. Greenberger, Overexpression of the human manganese superoxide dismutase (MnSOD) transgene in subclones of murine hematopoietic progenitor cell line 32D cl 3 decreases irradiation-induced apoptosis but does not alter G2/M or G1/S phase cell cycle arrest. *Radiat Oncol Investig* **7**, 331-342 (1999)10.1002/(SICI)1520-6823(1999)7:6<331::AID-ROI3>3.0.CO;2-M).
30. M. W. Epperly, J. A. Bray, S. Krager, L. M. Berry, W. Gooding, J. F. Engelhardt, R. Zwacka, E. L. Travis, J. S. Greenberger, Intratracheal injection of adenovirus containing the human MnSOD transgene protects athymic nude mice from irradiation-induced organizing alveolitis. *International journal of radiation oncology, biology, physics* **43**, 169-181 (1999); published online EpubJan 1 (S0360301698003551 [pii]).
31. A. A. Tarhini, C. P. Belani, J. D. Luketich, A. Argiris, S. S. Ramalingam, W. Gooding, A. Pennathur, D. Petro, K. Kane, D. Liggitt, T. ChampionSmith, X. Zhang, M. W. Epperly, J. S. Greenberger, A Phase I Study of Concurrent Chemotherapy (Paclitaxel and Carboplatin) and Thoracic Radiotherapy with Swallowed Manganese Superoxide Dismutase Plasmid Liposome Protection in Patients with Locally Advanced Stage III Non-Small-Cell Lung Cancer. *Human Gene Therapy* **22**, 336--342 (2011).
32. J. S. Greenberger, M. W. Epperly, J. Gretton, M. Jefferson, S. Nie, M. Bernarding, V. Kagan, H. L. Guo, Radioprotective gene therapy. *Curr Gene Ther* **3**, 183-195 (2003); published online EpubJun (
33. Z. Zhong, M. Froh, M. D. Wheeler, O. Smutney, T. G. Lehmann, R. G. Thurman, Viral gene delivery of superoxide dismutase attenuates experimental cholestasis-induced liver fibrosis in the rat. *Gene Therapy* **9**, 183--191 (2002).
34. T. G. Lehmann, M. D. Wheeler, M. Froh, R. F. Schwabe, H. Bunzendahl, R. J. Samulski, J. J. Lemasters, D. A. Brenner, R. G. Thurman, Effects of three superoxide dismutase genes delivered with an adenovirus

on graft function after transplantation of fatty livers in the rat. *Transplantation* **76**, 28-37 (2003); published online EpubJul 15 (10.1097/01.TP.0000065299.29900.17).
35. M. C. Vozenin-Brotons, F. Milliat, J. C. Sabourin, A. C. de Gouville, A. Francois, P. Lasser, P. Morice, C. Haie-Meder, A. Lusinchi, S. Antoun, J. Bourhis, D. Mathe, T. Girinsky, J. Aigueperse, Fibrogenic signals in patients with radiation enteritis are associated with increased connective tissue growth factor expression. *International journal of radiation oncology, biology, physics* **56**, 561-572 (2003); published online EpubJun 1 (
36. V. Haydont, B. L. Riser, J. Aigueperse, M. C. Vozenin-Brotons, Specific signals involved in the long-term maintenance of radiation-induced fibrogenic differentiation: a role for CCN2 and low concentration of TGF- 1. *AJP: Cell Physiology* **294**, C1332--C1341 (2008).
37. S. Hamama, S. Delanian, V. Monceau, M.-C. Vozenin, Therapeutic management of intestinal fibrosis induced by radiation therapy: from molecular profiling to new intervention strategies et vice et versa. *Fibrogenesis \& Tissue Repair* **5 Suppl 1**, S13 (2012).
38. K. L. Bennewith, X. Huang, C. M. Ham, E. E. Graves, J. T. Erler, N. Kambham, J. Feazell, G. P. Yang, A. Koong, A. J. Giaccia, The Role of Tumor Cell-Derived Connective Tissue Growth Factor (CTGF/CCN2) in Pancreatic Tumor Growth. *Cancer Research* **69**, 775--784 (2009).
39. B. Rooney, H. O'Donovan, A. Gaffney, M. Browne, N. Faherty, S. P. Curran, D. Sadlier, C. Godson, D. P. Brazil, J. Crean, CTGF/CCN2 activates canonical Wnt signalling in mesangial cells through LRP6: Implications for the pathogenesis of diabetic nephropathy. *FEBS Letters* **585**, 531--538 (2011).
40. S. Bickelhaupt, C. Erbel, C. Timke, U. Wirkner, M. Dadrich, P. Flechsig, A. Tietz, J. Pfohler, W. Gross, P. Peschke, L. Hoeltgen, H. A. Katus, H. J. Grone, N. H. Nicolay, R. Saffrich, J. Debus, M. D. Sternlicht, T. W. Seeley, K. E. Lipson, P. E. Huber, Effects of CTGF Blockade on Attenuation and Reversal of Radiation-Induced Pulmonary Fibrosis. *Journal of the National Cancer Institute* **109**, (2017); published online EpubAug 01 (10.1093/jnci/djw339).
41. R. Kadle, J. Cohen, W. Hambley, A. Gomez-Viso, W. Rifkin, R. Allen, N. Karp, P. Saadeh, D. Ceradini, J. Levine, T. Avraham, A 35-Year Evolution of Free Flap-Based Breast Reconstruction at a Large Urban Academic Center. *Journal of reconstructive microsurgery* **32**, 147-152 (2016); published online EpubFeb (10.1055/s-0035-1563702).
42. C. Healy, R. J. Allen, Sr., The evolution of perforator flap breast reconstruction: twenty years after the first DIEP flap. *Journal of reconstructive microsurgery* **30**, 121-125 (2014); published online EpubFeb (10.1055/s-0033-1357272).
43. R. Seth, A. A. Khan, T. Pencavel, K. J. Harrington, P. A. Harris, Targeted gene delivery by free-tissue transfer in oncoplastic reconstruction. *Lancet Oncology* **13**, e392--e402 (2012).
44. J. t. Michaels, M. Dobryansky, R. D. Galiano, D. J. Ceradini, R. Bonillas, D. Jones, N. Seiser, J. P. Levine, G. C. Gurtner, Ex vivo transduction of microvascular free flaps for localized peptide delivery. *Ann Plast Surg* **52**, 581-584 (2004); published online EpubJun (
45. J. t. Michaels, J. P. Levine, A. Hazen, D. J. Ceradini, R. D. Galiano, H. Soltanian, G. C. Gurtner, Biologic brachytherapy: ex vivo transduction of microvascular beds for efficient, targeted gene therapy. *Plast Reconstr Surg* **118**, 54-65; discussion 66-58 (2006); published online EpubJul (10.1097/01.prs.0000220466.27521.22).
46. M. P. Dempsey, C. Hamou, J. t. Michaels, S. Ghali, L. Jazayeri, R. H. Grogan, G. C. Gurtner, Using genetically modified microvascular free flaps to deliver local cancer immunotherapy with minimal systemic toxicity. *Plast Reconstr Surg* **121**, 1541-1553 (2008); published online EpubMay (10.1097/PRS.0b013e31816ff6aa).
47. R. Seth, A. A. Khan, T. D. Pencavel, M. J. Wilkinson, J. N. Kyula, G. Simpson, H. Pandha, A. Melcher, R. Vile, P. A. Harris, K. J. Harrington, Adenovirally delivered enzyme prodrug therapy with herpes simplex virus-thymidine kinase in composite tissue free flaps shows therapeutic efficacy in rat models of glioma. *Plast Reconstr Surg* **135**, 475-487 (2015); published online EpubFeb (10.1097/PRS.0000000000000878).
48. V. K. Agrawal, K. M. Copeland, Y. Barbachano, A. Rahim, R. Seth, C. L. White, M. Hingorani, C. M. Nutting, M. Kelly, P. Harris, H. Pandha, A. A. Melcher, R. G. Vile, C. Porter, K. J. Harrington, Microvascular free tissue transfer for gene delivery: in vivo evaluation of different routes of plasmid and adenoviral delivery. *Gene Ther* **16**, 78-92 (2009); published online EpubJan (gt2008140 [pii] 10.1038/gt.2008.140).
49. J. D. Cox, J. Stetz, T. F. Pajak, Toxicity criteria of the Radiation Therapy Oncology Group (RTOG) and the European Organization for Research and Treatment of Cancer (EORTC). *International journal of radiation oncology, biology, physics* **31**, 1341-1346 (1995); published online EpubMar 30 (10.1016/0360-3016(95)00060-C).
50. M. Neeman, A. A. Gilad, H. Dafni, B. Cohen, Molecular imaging of angiogenesis. *Journal of magnetic resonance imaging : JMRI* **25**, 1-12 (2007); published online EpubJan (10.1002/jmri.20774).

51. L. D. McPhail, S. P. Robinson, Intrinsic susceptibility MR imaging of chemically induced rat mammary tumors: relationship to histologic assessment of hypoxia and fibrosis. *Radiology* **254**, 110-118 (2010); published online EpubJan (10.1148/radiol.2541090395).
52. Y. Jamin, L. Glass, A. Hallsworth, R. George, D. M. Koh, A. D. Pearson, L. Chesler, S. P. Robinson, Intrinsic susceptibility MRI identifies tumors with ALKF1174L mutation in genetically-engineered murine models of high-risk neuroblastoma. *PLoS One* **9**, e92886 (2014)10.1371/journal.pone.0092886).
53. P. J. Taub, J. D. Marmur, W. X. Zhang, D. Senderoff, M. L. Urken, L. Silver, H. Weinberg, Effect of time on the viability of ischemic skin flaps treated with vascular endothelial growth factor (VEGF) cDNA. *Journal of reconstructive microsurgery* **14**, 387-390 (1998); published online EpubAug (10.1055/s-2007-1000196).
54. S. J. Russell, K. W. Peng, J. C. Bell, Oncolytic virotherapy. *Nature biotechnology* **30**, 658-670 (2012); published online EpubJul (10.1038/nbt.2287).
55. Y. Niu, H. Wang, D. Wiktor-Brown, R. Rugo, H. Shen, M. S. Huq, B. Engelward, M. Epperly, J. S. Greenberger, Irradiated Esophageal Cells are Protected from Radiation-Induced Recombination by MnSOD Gene Therapy. *Radiation Research* **173**, 453--461 (2010).
56. M. J. Perez, A. I. Cederbaum, Adenovirus-mediated expression of Cu/Zn- or Mn-superoxide dismutase protects against CYP2E1-dependent toxicity. *Hepatology* **38**, 1146-1158 (2003); published online EpubNov (10.1053/jhep.2003.50479).
57. V. Haydont, C. Bourgier, M. C. Vozenin-Brotons, Rho/ROCK pathway as a molecular target for modulation of intestinal radiation-induced toxicity. *British Journal of Radiology* **80**, S32--S40 (2007).
58. V. Haydont, C. Bourgier, M. Pocard, A. Lusinchi, J. Aigueperse, D. Mathe, J. Bourhis, M. C. Vozenin-Brotons, Pravastatin Inhibits the Rho/CCN2/extracellular matrix cascade in human fibrosis explants and improves radiation-induced intestinal fibrosis in rats. *Clinical cancer research : an official journal of the American Association for Cancer Research* **13**, 5331-5340 (2007); published online EpubSep 15 (10.1158/1078-0432.CCR-07-0625).
59. M. Wang, J. S. Kirk, S. Venkataraman, F. E. Domann, H. J. Zhang, F. Q. Schafer, S. W. Flanagan, C. J. Weydert, D. R. Spitz, G. R. Buettner, L. W. Oberley, Manganese superoxide dismutase suppresses hypoxic induction of hypoxia-inducible factor-1alpha and vascular endothelial growth factor. *Oncogene* **24**, 8154-8166 (2005); published online EpubDec 08 (10.1038/sj.onc.1208986).
60. L. W. Oberley, Mechanism of the tumor suppressive effect of MnSOD overexpression. *Biomedicine & pharmacotherapy = Biomedecine & pharmacotherapie* **59**, 143-148 (2005); published online EpubMay (10.1016/j.biopha.2005.03.006).
61. S. Venkataraman, X. Jiang, C. Weydert, Y. Zhang, H. J. Zhang, P. C. Goswami, J. M. Ritchie, L. W. Oberley, G. R. Buettner, Manganese superoxide dismutase overexpression inhibits the growth of androgen-independent prostate cancer cells. *Oncogene* **24**, 77-89 (2005); published online EpubJan 06 (10.1038/sj.onc.1208145).
62. S. K. Dhar, J. Tangpong, L. Chaiswing, T. D. Oberley, D. K. St Clair, Manganese Superoxide Dismutase Is a p53-Regulated Gene That Switches Cancers between Early and Advanced Stages. *Cancer Research* **71**, 6684--6695 (2011).
63. A. R. Cyr, M. J. Hitchler, F. E. Domann, Regulation of SOD2 in cancer by histone modifications and CpG methylation: closing the loop between redox biology and epigenetics. *Antioxidants & redox signaling* **18**, 1946-1955 (2013); published online EpubMay 20 (10.1089/ars.2012.4850).
64. J. H. Kim, A. J. J. Kolozsvary, K. A. Jenrow, S. L. Brown, Mechanisms of radiation-induced skin injury and implications for future clinical trials. *International Journal of Radiation Biology* **89**, 311--318 (2013).
65. N. S. Russell, S. Hoving, S. Heeneman, J. J. Hage, L. A. E. Woerdeman, R. de Bree, P. J. F. M. Lohuis, L. Smeele, J. Cleutjens, A. Valenkamp, L. D. A. Dorresteijn, O. Dalesio, M. J. Daemen, F. A. Stewart, Novel insights into pathological changes in muscular arteries of radiotherapy patients. *Radiotherapy and Oncology* **92**, 477--483 (2009).
66. B. Jolles, R. G. Harrison, Enzymic processes and vascular changes in the skin radiation reaction. *The British journal of radiology* **39**, 12-18 (1966); published online EpubJan (
67. R. S. Jaenke, M. E. Robbins, T. Bywaters, E. Whitehouse, M. Rezvani, J. W. Hopewell, Capillary endothelium. Target site of renal radiation injury. *Laboratory investigation; a journal of technical methods and pathology* **68**, 396-405 (1993); published online EpubApr (
68. D. G. Baker, R. J. Krochak, The response of the microvascular system to radiation: a review. *Cancer investigation* **7**, 287-294 (1989).
69. M. H. Janssen, H. J. Aerts, R. G. Kierkels, W. H. Backes, M. C. Ollers, J. Buijsen, P. Lambin, G. Lammering, Tumor perfusion increases during hypofractionated short-course radiotherapy in rectal cancer: sequential perfusion-CT findings. *Radiother Oncol* **94**, 156-160 (2010); published online EpubFeb (10.1016/j.radonc.2009.12.013).

70. D. Danielsson, K. Brehwens, M. Halle, M. Marczyk, A. Sollazzo, J. Polanska, E. Munck-Wikland, A. Wojcik, S. Haghdoost, Influence of genetic background and oxidative stress response on risk of mandibular osteoradionecrosis after radiotherapy of head and neck cancer. *Head Neck*, (2014); published online EpubOct 28 (10.1002/hed.23903).
71. M. W. Epperly, H. Guo, D. Shields, X. Zhang, J. S. Greenberger, Correlation of ionizing irradiation-induced late pulmonary fibrosis with long-term bone marrow culture fibroblast progenitor cell biology in mice homozygous deletion recombinant negative for endothelial cell adhesion molecules. *In Vivo* **18**, 1-14 (2004); published online EpubJan-Feb (
72. V. K. Agrawal, K. M. Copeland, Y. Barbachano, A. Rahim, R. Seth, C. L. White, M. Hingorani, C. M. Nutting, M. Kelly, P. Harris, H. Pandha, A. A. Melcher, R. G. Vile, C. Porter, K. J. Harrington, Microvascular free tissue transfer for gene delivery: in vivo evaluation of different routes of plasmid and adenoviral delivery. *Gene Therapy* **16**, 78--92 (2008).
73. S. Walker-Samuel, M. Orton, L. D. McPhail, J. K. Boult, G. Box, S. A. Eccles, S. P. Robinson, Bayesian estimation of changes in transverse relaxation rates. *Magnetic resonance in medicine* **64**, 914-921 (2010); published online EpubSep (10.1002/mrm.22478).
74. L. C. Baker, J. K. Boult, Y. Jamin, L. D. Gilmour, S. Walker-Samuel, J. S. Burrell, M. Ashcroft, F. A. Howe, J. R. Griffiths, J. A. Raleigh, A. J. van der Kogel, S. P. Robinson, Evaluation and immunohistochemical qualification of carbogen-induced DeltaR(2) as a noninvasive imaging biomarker of improved tumor oxygenation. *International journal of radiation oncology, biology, physics* **87**, 160-167 (2013); published online EpubSep 1 (10.1016/j.ijrobp.2013.04.051).
75. J. W. Bainbridge, C. Stephens, K. Parsley, C. Demaison, A. Halfyard, A. J. Thrasher, R. R. Ali, In vivo gene transfer to the mouse eye using an HIV-based lentiviral vector; efficient long-term transduction of corneal endothelium and retinal pigment epithelium. *Gene Ther* **8**, 1665-1668 (2001); published online EpubNov (10.1038/sj.gt.3301574).